

EFFICIENT AND INTERPRETABLE ADDITIVE GAUSSIAN PROCESS REGRESSION AND APPLICATION TO ANALYSIS OF HOURLY-RECORDED NO₂ CONCENTRATIONS IN LONDON

BY SAHOKO ISHIDA^{1,a} AND WICHER BERGSMA^{1,b}

¹*Department of Statistics, London School of Economics and Political Science, ^as.ishida@lse.ac.uk; ^bw.p.bergsma@lse.ac.uk*

This paper focuses on interpretable additive Gaussian process (GP) regression and its efficient implementation for large-scale data with a multi-dimensional grid structure, as commonly encountered in spatio-temporal analysis. A popular and scalable approach in the GP literature for this type of data exploits the Kronecker product structure in the covariance matrix. However, under the existing methodology, its use is limited to covariance functions with a separable product structure, which lacks flexibility in modelling and selecting interaction effects - an important component in many real-life problems. To address these issues, we propose a class of additive GP models constructed by hierarchical ANOVA kernels. Furthermore, we show that how the Kronecker method can be extended to the proposed class of models. Our approach allows for easy identification of interaction effects, straightforward interpretation of both main and interaction effects and efficient implementation for large-scale data. The proposed method is applied to analyse NO₂ concentrations during the COVID-19 lockdown in London. Our scalable method enables analysis of hourly-recorded data collected from 59 different stations across the city, providing additional insights to findings from previous research using daily or weekly averaged data.

1. Introduction. Gaussian process (GP) regression is a popular method in machine learning, with its kernel playing a vital role in capturing relationships between predictors and the response variable. GPs offer flexibility in modeling complex relationships through variety of kernel options, and effectively handle auto-correlated data. This characteristic makes GPs particularly well-suited for applications in fields like epidemiology and environmental science, where accounting for auto-correlation in spatial and temporal domains is essential. GP regression has a long history in spatial and spatio-temporal analysis and is closely connected to well-established methods such as Kriging (Krige, 1951; Matheron, 1963) for geostatistical data, log-Gaussian Cox processes (Møller, Syversveen and Waagepetersen, 1998) for modelling spatial and spatio-temporal point processes (Diggle et al., 2013) and a family of conditional auto-regressive models for areal data (see Lee (2011) for an overview).

Environmental monitoring and forecasting has benefited from the development of GP regression (Grancharova, Kocijan and Johansen, 2008; Petelin, Grancharova and Kocijan, 2013; Datta et al., 2016; Liu et al., 2018; Patel et al., 2022; Pinder et al., 2021). With the COVID-19 pandemic, air quality monitoring has gained renewed attention as the lockdown measures have led to changes in traffic and industrial activities, the major sources of air pollutant emissions. Researchers have used data collected from monitoring sites in different regions and various statistical methods, including GP regression, to investigate the impact of restricted mobility on air quality. Examples of such studies include Solberg et al. (2021), Fioravanti et al. (2022), Lee et al. (2020), and Cameletti (2020).

Keywords and phrases: Gaussian process regression, Spatio-temporal analysis, Kronecker products, Air quality monitoring.

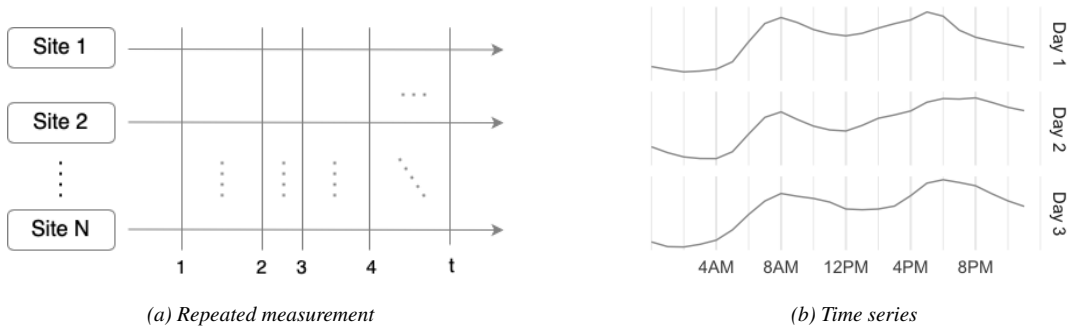


Fig 1: Example of data with multidimensional grid structure. The left panel is an example of repeated measurements from different sites. Notably, timestamps need not be evenly spaced. This example can also be seen as a series of time series. The right panel illustrates that each time series with periodicity (e.g. daily cycle) also has a two-dimensional grid structure.

1.1. *Hourly-recorded nitrogen dioxide concentrations in London.* In this paper, we analyze a large dataset of hourly-recorded nitrogen dioxide (NO_2) concentrations in London, comprising over 200,000 data points from 59 air quality monitoring stations over 147 days (January 6th to May 31st, 2020). Due to spatial, temporal, and periodic patterns in the data, we utilize additive GP models (Plate, 1999; Duvenaud, Nickisch and Rasmussen, 2011) to account for these patterns and potential interaction effects. These models assume an additive structure of GPs for the regression function, akin to generalized additive models (Hastie and Tibshirani, 1990). We denote the response variable, i.e., the NO_2 concentration, at monitoring station s , on day d , and at hour h , as $y_{s,d,h}$. We consider a model given by

$$y_{s,d,h} = f(\mathbf{x}_{1s}, x_{2d}, x_{3h}) + \epsilon_{s,d,h} \quad (1.1)$$

where $\epsilon_{s,d,h}$ is an error term, and $\mathbf{x}_{1s}, x_{2d}, x_{3h}$ represents the three predictors: two dimensional geo-graphical coordinate of station s , day number d and hour of the day h . The specification of $f(\mathbf{x}_{1s}, x_{2d}, x_{3h})$ depends on the model assumptions. An example is given by

$$f(\mathbf{x}_{1s}, x_{2d}, x_{3h}) = a + f_1(\mathbf{x}_{1s}) + f_2(x_{2d}) + f_3(x_{3h}) \\ + f_{12}(\mathbf{x}_{1s}, x_{2d}) + f_{13}(\mathbf{x}_{1s}, x_{3h}) + f_{23}(x_{2d}, x_{3h}). \quad (1.2)$$

In this example, the first term after the constant a captures spatial patterns, while the second and third terms model the global time trend and daily cyclical effect, respectively. In addition to these main effects, we include two-way interaction terms to capture how these effects vary across space and time. For example, the last term $f_{23}(x_{2d}, x_{3h})$ accounts for the interaction effect between *global time* and *hour of the day*, reflecting the belief that the daily cycle changes over time. Additive GP models assume that each function in (1.2) follows a GP. We can explore simpler models with only main terms or a subset of interaction effects. If all two-way interactions are present, we can consider adding the three-way interaction effect $f_{123}(\mathbf{x}_{1s}, x_{2d}, x_{3h})$, which gives a saturated model. Section 4.2 lists all models considered for this dataset. While intuitively reasonable, additive GP models have not been extensively explored for analyzing hourly-recorded air quality measurements of this size.

1.2. *Methodological challenges and our contributions.* Current methodologies for additive GP models face two challenges: interpretation and computation. Interpretation of a regression model is an essential part of analysing real-world data. Plate (1999) is one of the first to discuss the importance of modelling interactions and a trade-off between interpretability and accuracy in flexible modelling using GP, which can be done through kernel

construction. [Duvenaud, Nickisch and Rasmussen \(2011\)](#) is a more recent attempt at kernel-based modelling of main and interaction effects. The key idea lies in constructing interaction effect terms using the provided kernels for main effects. However, the proposed methodology does not guarantee certain common practices in statistical modeling, such as a hierarchical structure in interaction terms. In the presence of higher-order interactions, further discussion is warranted regarding the interpretation of main and lower-order interaction effects within the proposed model.

To address this issue, we adopt the idea of the *ANOVA decomposition kernel* ([Stitson et al., 1999](#); [Durrande et al., 2013](#)). Using this class of kernels in GP regression implies assuming saturated model, i.e., model with main terms and all interaction terms up to the highest orders, which may be too restrictive. This paper uses the *hierarchical ANOVA decomposition kernel* ([Bergsma and Jamil, 2023](#)) which accommodates a broader class of regression models with main effects and selected interaction effects. As with any statistical modelling problem, interaction terms are included along with main terms and any lower-order interaction terms. Additionally, we incorporate centring of kernels when constructing the hierarchical ANOVA decomposition kernel to facilitate the interpretability of the results. After centring, all terms in the model, including the main and lower-order interaction effects, possess an intuitive interpretation.

However, implementing such flexible GP models poses computational challenges due to time complexity $O(n^3)$ and storage requirement $O(n^2)$. Air quality monitoring data, collected from multiple measurement stations over long periods, often results in a large number of data points, making standard GP regression impractical. As a result, environmental monitoring studies often scale down the data by limiting the number of measurement sites or modeling daily or weekly averaged data. There are various approaches to reduce the computational burden of GP models (see [Liu et al. \(2020\)](#) for an overview). One particularly effective approach is to make use of a Kronecker product structure in covariance matrix, which is applicable when the data has a multidimensional grid structures. This can also be understood as multi-level panel data commonly found in environmental monitoring. For example, measurements from different monitoring stations recorded at the same timestamps form a two-dimensional grid. Interestingly, single time series data with periodicity, such as the daily cycle commonly observed in ambient air pollutant concentrations, can also be treated as two-dimensional grid data. [Figure 1](#) illustrates these examples. As shown in the previous work by [Flaxman et al. \(2015\)](#); [Wilson et al. \(2014\)](#); [Saatçi \(2012\)](#); [Gilboa, Saatçi and Cunningham \(2013\)](#), the Kronecker method reduces computational complexity and storage requirement to $O(n)$ in the best case, without relying on approximations. However, these methods were limited to specific submodels, such as saturated models or those with only the highest-ordered interaction terms. This implies that other additive models, such as main effect or non-saturated interaction effect models, still face constraints with $O(n^3)$ computations and $O(n^2)$ storage, or require the use of other scalable methods that rely on approximations (See [Section 3.5](#) for a brief summary). While these methods avoid imposing restrictions on kernel structure, they typically do not enjoy the same scalability and accuracy of the Kronecker method.

This paper introduces an extension of the Kronecker method, specifically designed to handle any models constructed using the hierarchical ANOVA kernel, wherein the centring of kernels plays a crucial role. This novel Kronecker approach enables the modelling of larger-scale data with many structures, including, but not limited to, saturated models.

We applied the proposed method to analyse the previously mentioned NO_2 concentration data. The structure of the dataset can be viewed as a combination of the two examples shown in [Figure 1a](#) and [1b](#), resulting in a three-dimensional grid structure (as depicted in [Figure 2](#)) with monitoring station, calendar date, and hour of the day as the top-level, middle-level, and bottom-level, respectively. This allowed us to efficiently implement the models with various

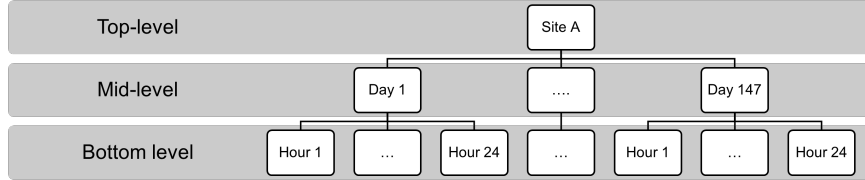


Fig 2: The structure of the NO_2 dataset

structures. Our data analysis, which used hourly-recorded data collected from 59 stations over 21 weeks, identified spatial, temporal, and periodic patterns in the data and how they interact with each other. These patterns and effects can easily be visualised and interpreted.

1.3. *Organization of the work.* The paper is organized as follows: Section 2 introduces the proposed additive GP models with hierarchical ANOVA kernels, including the concept of centring of kernels. In Section 3, we present our approach for efficiently implementing the proposed model for multi-dimensional grid structured data, leveraging the Kronecker product structure in the model covariance matrix. We primarily focus on two-dimensional grid data and two-predictor models as the main motivating example, since the concepts and advantages can be effectively illustrated in this simple setting. Each section also provides a generalization to higher-dimensional cases. Section 4 delves into the details of our specific application, including data description, model formulation, results, and their interpretation.

2. Additive Gaussian process model. Let \mathcal{X}_1 and \mathcal{X}_2 be nonempty sets. Consider a regression model for a real-valued response y and two predictors $\mathbf{x}_1 \in \mathcal{X}_1, \mathbf{x}_2 \in \mathcal{X}_2$. In the example in Figure 1a, \mathbf{x}_1 and \mathbf{x}_2 can be the location of the sites expressed in a set of coordinates and a timestamp. If the data is expressed in a long format and n is the total number of observations, for $i = 1, \dots, n$, the model is expressed as

$$y_i = f(\mathbf{x}_{1i}, \mathbf{x}_{2i}) + \epsilon_i \quad (2.1)$$

where the error terms $(\epsilon_1, \dots, \epsilon_n) \sim \text{MVN}(\mathbf{0}, \Sigma)$. For i.i.d errors, we write $\Sigma = \sigma^2 \mathbf{I}_n$ where \mathbf{I}_n is the $n \times n$ identity matrix. Given two predictors and a constant a , it is natural to consider following additive models:

$$f(\mathbf{x}_{1i}, \mathbf{x}_{2i}) = a + f_1(\mathbf{x}_{1i}) + f_2(\mathbf{x}_{2i}) \quad (2.2)$$

$$f(\mathbf{x}_{1i}, \mathbf{x}_{2i}) = a + f_1(\mathbf{x}_{1i}) + f_2(\mathbf{x}_{2i}) + f_{12}(\mathbf{x}_{1i}, \mathbf{x}_{2i}). \quad (2.3)$$

While the first represents the main effect model, the second assumes an additional interaction effect between the two predictors. The main idea of additive GP models is to put a GP prior on each function f_1, f_2 and f_{12} in (2.2) and (2.3). The model formulation above is not restricted to the two-dimensional grid structure and it is applicable to any regression problems with two predictors. We will re-formulate the same models in Section 3 for two-dimensional grid structure data and show how the necessary computation can be made efficient. In this section, we will discuss statistical modelling with a GP prior.

2.1. *Gaussian processes and kernels.* The key component of a GP is its covariance function, known as the *kernel*. In what follows we define kernel and GP.

DEFINITION 1 (Kernel). Let \mathcal{X} be a nonempty set. A symmetric function $k : \mathcal{X} \times \mathcal{X} \rightarrow \mathbb{R}$ is called *positive definite kernel*, or simply *kernel*, if for all $n = 1, 2, \dots$, $a_1, \dots, a_n \in \mathbb{R}$ and $\mathbf{x}_1, \dots, \mathbf{x}_n \in \mathcal{X}$, $\sum_{i=1}^n \sum_{j=1}^n a_i a_j k(\mathbf{x}_i, \mathbf{x}_j) \geq 0$.

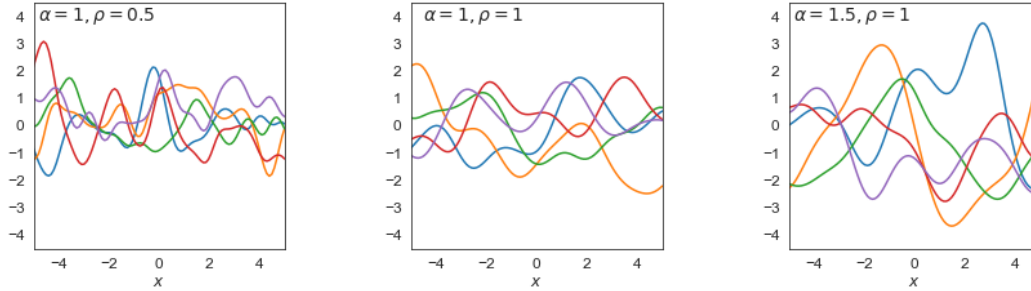


Fig 3: Sample paths from zero mean Gaussian process with 1-dimensional squared exponential kernel. The y -axis is $y = f(x)$. Taking the middle panel as reference, the left panel has smaller length scale which makes the process more wiggly. Having a larger sample scale parameter (right panel) makes the average distance from the mean(0) bigger.

DEFINITION 2 (Gaussian Process). Let \mathcal{X} be a non-empty set, $k : \mathcal{X} \times \mathcal{X} \rightarrow \mathbb{R}$ be a (positive definite) kernel, and $m : \mathcal{X} \rightarrow \mathbb{R}$ be a real-valued function. A random function $f : \mathcal{X} \rightarrow \mathbb{R}$ is a Gaussian Process with mean function m and kernel k , if, for any finite set $\mathbf{x}_i \in \mathcal{X}$ for $i = 1, \dots, n$, the random vector $\mathbf{f} = (f(\mathbf{x}_1), \dots, f(\mathbf{x}_n))^\top$ follows multivariate Gaussian distribution $\text{MVN}(\mathbf{m}, \mathbf{K})$ where $\mathbf{m} = (m(\mathbf{x}_1), \dots, m(\mathbf{x}_n))^\top$ and \mathbf{K} is a $n \times n$ matrix with (i, j) -th element given by $k(\mathbf{x}_i, \mathbf{x}_j)$.

Throughout the paper, we denote a random function f following a Gaussian process (GP) with a mean function m and a kernel k by $f \sim \text{GP}(m, k)$. The matrix \mathbf{K} is referred to as the Gram matrix. The GP is fully specified by its mean function and kernel, allowing us to incorporate our beliefs about the regression function. In the absence of prior beliefs, a common choice is to set the mean function as zero, i.e., $m(x) = 0$ for all $x \in \mathcal{X}$. Under this assumption, the kernel k defines a unique GP, and selecting a specific kernel corresponds to making different assumptions about the underlying process. For instance, the squared exponential (SE) kernel (2.4) is widely used in machine learning and associated with a very smooth process that possesses mean-square derivatives of all orders (Adler (1981, Chapter 2)).

EXAMPLE 1 (Squared exponential kernel). Let $\mathcal{X} \subset \mathbb{R}^p$. For $\alpha > 0$ and $\rho > 0$, a squared exponential (SE) kernel $k_{se} : \mathcal{X} \times \mathcal{X} \rightarrow \mathbb{R}$ is defined by

$$k_{se}(\mathbf{x}, \mathbf{x}') = \alpha^2 \exp\left(-\frac{\|\mathbf{x} - \mathbf{x}'\|^2}{2\rho^2}\right), \quad \mathbf{x}, \mathbf{x}' \in \mathcal{X}. \quad (2.4)$$

We refer to unknown parameters in a kernel as hyper-parameters. In the example above, we have a scale parameter α and a length-scale parameter ρ . The values of these hyper-parameters also carry assumptions on the underlying process. See Figure 3 for a further demonstration of this. We show a few of the other popular kernels in machine learning and spatial statistics in Section 1.1 of the Supplementary Material (Ishida and Bergsma, 2023). For more comprehensive reviews on different classes of kernels, see Rasmussen and Williams (2006, Chapter 4) and Genton (2001) for example.

2.2. Statistical modelling with kernels.

2.2.1. *Sum kernels and main effect terms.* Let us revisit the main effect model with 2 predictors specified in (2.1) and (2.2). Given two kernels $k_1 : \mathcal{X}_1 \times \mathcal{X}_1 \rightarrow \mathbb{R}$ and $k_2 : \mathcal{X}_2 \times \mathcal{X}_2 \rightarrow \mathbb{R}$, we assume $f_1 \sim \text{GP}(0, k_1)$ and $f_2 \sim \text{GP}(0, k_2)$. A nice property of kernels is that the sum of the given two valid kernels constitutes a new kernel. With the additional assumption that the constant term $a \sim N(0, 1)$, the overall function $f : \mathcal{X} \rightarrow \mathbb{R}$ with $\mathcal{X} = \mathcal{X}_1 \times \mathcal{X}_2$ follows $\text{GP}(0, k)$ where $k : \mathcal{X} \times \mathcal{X} \rightarrow \mathbb{R}$ is given by

$$k((\mathbf{x}_1, \mathbf{x}_2), (\mathbf{x}'_1, \mathbf{x}'_2)) = 1 + k_1(\mathbf{x}_1, \mathbf{x}'_1) + k_2(\mathbf{x}_2, \mathbf{x}'_2).$$

Note that the first term 1 is also a positive definite kernel, known as a constant kernel, hence the function k can be seen as a sum of three positive definite kernels. To avoid constraining the prior variance of the constant term a , we multiply the overall kernel k by α_0^2 where $\alpha_0 > 0$, i.e.,

$$k((\mathbf{x}_1, \mathbf{x}_2), (\mathbf{x}'_1, \mathbf{x}'_2)) = \alpha_0^2 (1 + k_1(\mathbf{x}_1, \mathbf{x}'_1) + k_2(\mathbf{x}_2, \mathbf{x}'_2)).$$

With this formulation, we assume $a \sim N(0, \alpha_0^2)$, and the scale parameters of k_1 and k_2 , (denoted by α_1^2 and α_2^2), are re-scaled by the factor of α_0^2 . The corresponding Gram matrix is given by

$$\mathbf{K} = \alpha_0^2 \left(\mathbf{1}_n \mathbf{1}_n^\top + \mathbf{K}_1 + \mathbf{K}_2 \right)$$

where $\mathbf{1}_n \mathbf{1}_n^\top$ is a $n \times n$ matrix with all elements equal to 1, and \mathbf{K}_l is a Gram matrix with i, j -th element given by $k_l(\mathbf{x}_i, \mathbf{x}'_j)$. We can generalize this to the case where with d predictors $\mathbf{x}_1, \dots, \mathbf{x}_d$.

EXAMPLE 2 (Main effect kernel). *Let \mathcal{X}_l be a nonempty set and k_l be a positive definite kernel on $\mathcal{X}_l \times \mathcal{X}_l$ for $l = 1, \dots, d$. Let $\mathcal{X} = \mathcal{X}_1, \dots, \mathcal{X}_d$. Given d predictors, the kernel that gives a main effect GP model is defined on $\mathcal{X} \times \mathcal{X}$ and given by*

$$k_{\text{main}}((\mathbf{x}_1, \dots, \mathbf{x}_d), (\mathbf{x}'_1, \dots, \mathbf{x}'_d)) = \alpha_0^2 \left(1 + \sum_{l=1}^d k_l(\mathbf{x}_l, \mathbf{x}'_l) \right), \quad \mathbf{x}_l, \mathbf{x}'_l \in \mathcal{X}_l. \quad (2.5)$$

2.2.2. *Tensor product kernels and interaction effect terms.* The interaction effect model (2.3) has an additional function term f_{12} . We put a zero mean GP prior on this, with its kernel $k : \mathcal{X} \times \mathcal{X} \rightarrow \mathbb{R}$ given by a tensor product of two kernels k_1 and k_2 . Formally, we have $k = k_1 \otimes k_2$ defined by $k((\mathbf{x}_1, \mathbf{x}_2), (\mathbf{x}'_1, \mathbf{x}'_2)) = k_1(\mathbf{x}_1, \mathbf{x}'_1)k_2(\mathbf{x}_2, \mathbf{x}'_2)$ where \otimes is a tensor product operator. Generalising this kernel to the case involving d predictors, we have the following definition.

DEFINITION 3 (Tensor product kernel). *Let \mathcal{X}_l be a nonempty set and k_l be a positive definite kernel on $\mathcal{X}_l \times \mathcal{X}_l$ for $l = 1, \dots, d$. With $\mathcal{X} = \mathcal{X}_1 \times \dots \times \mathcal{X}_d$, a tensor product of $\{k_l\}_{l=1}^d$ is a kernel on $\mathcal{X} \times \mathcal{X}$ defined as*

$$(\otimes_{l=1}^d k_l)((\mathbf{x}_1, \dots, \mathbf{x}_d), (\mathbf{x}'_1, \dots, \mathbf{x}'_d)) = \prod_{l=1}^d k_l(\mathbf{x}_l, \mathbf{x}'_l), \quad \mathbf{x}_l, \mathbf{x}'_l \in \mathcal{X}_l. \quad (2.6)$$

Using the sum kernel for the main effect terms, and the tensor product kernel for the interaction effect term, we can specify the prior on the regression function f in (2.3) as $\text{GP}(0, k)$, where $k = \alpha_0^2(1 + k_1 + k_2 + k_1 \otimes k_2)$ is defined by

$$k((\mathbf{x}_1, \mathbf{x}_2), (\mathbf{x}'_1, \mathbf{x}'_2)) = \alpha_0^2 (1 + k_1(\mathbf{x}_1, \mathbf{x}'_1) + k_2(\mathbf{x}_2, \mathbf{x}'_2) + k_1(\mathbf{x}_1, \mathbf{x}'_1)k_2(\mathbf{x}_2, \mathbf{x}'_2)). \quad (2.7)$$

The corresponding Gram matrix can be written as

$$\mathbf{K} = \alpha_0^2 \left(\mathbf{1}_n \mathbf{1}_n^\top + \mathbf{K}_1 + \mathbf{K}_2 + \mathbf{K}_1 \circ \mathbf{K}_2 \right)$$

where \circ is the element-wise product operator.

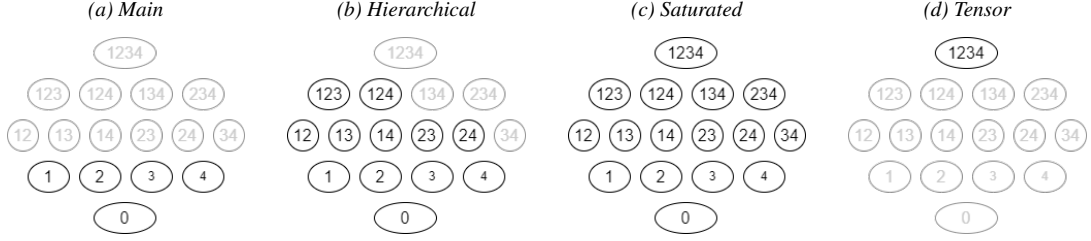


Fig 4: Visualisation of ANOVA decomposition kernels (Panel (a),(b) and (c)) and a tensor product kernel (Panel (d)) with $d = 4$ dimensional covariates. The term 0 in the panels refers to the constant term, and the terms 1 to 4 refers to main effect term that corresponds to k_l for $l = 1, \dots, 4$. The remaining terms are interaction effect terms, e.g., the term 123 models the three-way interaction effect involving the covariates $\mathbf{x}_1, \mathbf{x}_2$ and \mathbf{x}_3 . Panel (b) is an example of a hierarchical ANOVA decomposition kernel. Adding the term 34 to this example gives another example of such kernel. If we are to include the term 134 and/or 234, the term 34 should also be added in order to ensure a hierarchical structure.

2.2.3. *ANOVA decomposition kernel.* When including interaction terms in a model, it is a common practice to include both the main terms and any lower order interaction terms. In this section we introduce a special class of additive kernels, known as the ANOVA decomposition kernel, that can naturally take this into consideration. For a model with d predictors, we define a saturated ANOVA decomposition kernel as follows.

DEFINITION 4 (Saturated ANOVA decomposition kernel). *Let \mathcal{X}_l be a nonempty set, k_l be a positive definite kernel on $\mathcal{X}_l \times \mathcal{X}_l$ for $l = 1, \dots, d$ and α_0 be a positive constant. With $\mathcal{X} = \mathcal{X}_1 \times \dots \times \mathcal{X}_d$, the saturated ANOVA decomposition kernel $k_{s-anova} : \mathcal{X} \times \mathcal{X} \rightarrow \mathbb{R}$ is given by:*

$$k_{s-anova}((\mathbf{x}_1, \dots, \mathbf{x}_l), (\mathbf{x}'_1, \dots, \mathbf{x}'_l)) = \alpha_0^2 \prod_{l=1}^d (1 + k_l(\mathbf{x}_l, \mathbf{x}'_l)), \quad \mathbf{x}_l, \mathbf{x}'_l \in \mathcal{X}_l. \quad (2.8)$$

The (saturated) ANOVA decomposition kernel was first introduced by [Stitson et al. \(1999\)](#) in the context of Support Vector Machines. It borrows the idea of an ANOVA decomposition of a function in a Reproducing Kernel Hilbert Space (RKHS) ([Gu, 2002](#); [Wahba et al., 1995](#)). This kernel has 2^d terms, including a constant term, all of the base kernels, the d -th order interaction term and any lower order interaction terms. The kernel given by (2.7) is in fact this class of kernel. It can also be seen as a special case of tensor product kernels, by treating $\tilde{k}(\mathbf{x}_l, \mathbf{x}'_l) = 1 + k_l(\mathbf{x}_l, \mathbf{x}'_l)$ as one kernel. In contrast to the saturated ANOVA decomposition kernel, a GP model with a tensor product kernel in its simplest form given by Definition 3 only includes the highest interaction term. As we will see in the following sections, this may lead to a poor fit, and cause difficulty in interpretation of the fitted model. The saturated ANOVA kernel, however, assumes the highest complexity given a set of base kernels, which may be an over-fit to the data.

Therefore, we introduce another class of ANOVA decomposition kernels, called the *hierarchical ANOVA decomposition kernel*. This kernel includes a constant term, all main terms, and any interaction terms of any orders constructed using tensor product kernels. This means that no new kernels are introduced for interaction terms, and for given data, all models under this class of kernels share the same hyper-parameters. Additionally, this kernel must have a hierarchical structure, meaning that if we include any p -th order interaction terms, any lower order interaction terms involving any covariates used in the p -th order interaction terms must also be included. The smallest kernel in this class is the main effect kernel given by (2.5), and

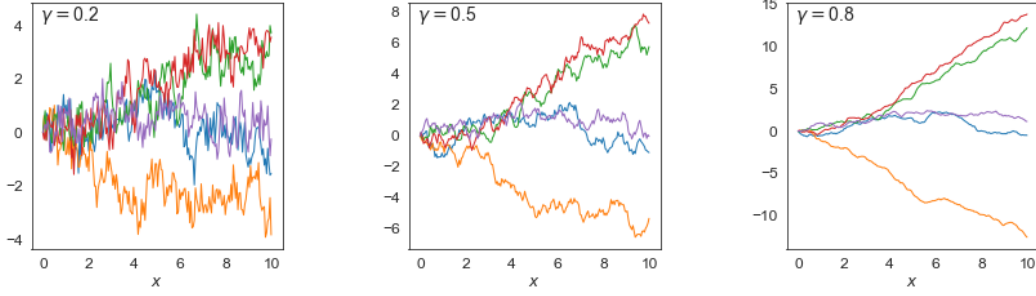


Fig 5: Sample paths ($y = f(x)$) from fBM kernel given in (2.11) with different values for Hurst coefficient γ .

the largest kernel is simply the saturated ANOVA decomposition kernel. Figure 4 illustrates the differences between the kernels discussed in this section with $d = 4$. It is worth noting that there are many hierarchical ANOVA kernels, and Figure 4b shows one such example.

2.3. Centring of kernels. Gaussian process paths may be arbitrary positioned, in which case, centring of kernels can be applied. A positive definite kernel can be centred by the following.

DEFINITION 5 (Centred kernel). *Let P be a probability distribution over a non empty set \mathcal{X} and $X, X' \sim P$ are independent. Any kernel $k : \mathcal{X} \times \mathcal{X} \rightarrow \mathbb{R}$ may be centred by*

$$k_{cent}(\mathbf{x}, \mathbf{x}') = \mathbb{E}_P [k(\mathbf{x}, \mathbf{x}') - k(\mathbf{x}, X) - k(\mathbf{x}', X') + k(X, X')], \quad \mathbf{x}, \mathbf{x}' \in \mathcal{X}. \quad (2.9)$$

A kernel centred by the above retains positive definiteness (see Section 2 of the Supplementary Material (Ishida and Bergsma, 2023)). In practice, we can use the empirical distribution of data $\mathbf{x}_1, \dots, \mathbf{x}_n$ to approximate the unknown P , i.e.,

$$k_{cent}(\mathbf{x}, \mathbf{x}') = k(\mathbf{x}, \mathbf{x}') - \frac{1}{n} \sum_{i=1}^n k(\mathbf{x}, \mathbf{x}_i) - \frac{1}{n} \sum_{j=1}^n k(\mathbf{x}', \mathbf{x}_j) + \frac{1}{n^2} \sum_{i=1}^n \sum_{j=1}^n k(\mathbf{x}_i, \mathbf{x}_j). \quad (2.10)$$

This ensures the function f evaluated at $\mathbf{x}_1, \dots, \mathbf{x}_n$ sums to zero, i.e., $\sum_{i=1}^n f(\mathbf{x}_i) = 0$. The empirically centred Gram matrix for a given \mathbf{K} , can be computed using a centring matrix $\mathbf{C} = \mathbf{I}_n - \frac{1}{n} \mathbf{1}_n \mathbf{1}_n^\top$, by $\mathbf{K}^{(c)} = \mathbf{C} \mathbf{K} \mathbf{C}$. This means that all columns and rows of $\mathbf{K}^{(c)}$ sum to 0. Centring of a kernel plays a key role in interpretation and efficient computation as shown in Section 2.4.2 and 3.3.

Centring example with fractional Brownian motion kernel. We will illustrate centring of kernels using fractional Brownian Motion (fBM) kernel.

EXAMPLE 3 (fractional Brownian motion kernel). *Let $\mathcal{X} \subset \mathbb{R}^p$ be a set. For $\alpha > 0$ and $0 < \gamma < 1$, the fractional Brownian motion kernel $k_{fBM_\gamma} : \mathcal{X} \times \mathcal{X} \rightarrow \mathbb{R}$ is given by*

$$k_{fBM_\gamma}(\mathbf{x}, \mathbf{x}') = \frac{\alpha^2}{2} (\|\mathbf{x}\|^{2\gamma} + \|\mathbf{x}'\|^{2\gamma} - \|\mathbf{x} - \mathbf{x}'\|^{2\gamma}), \quad \mathbf{x}, \mathbf{x}' \in \mathcal{X} \quad (2.11)$$

The Hurst coefficient γ in (2.11) determines the roughness of the process. A smaller value of γ is associated with rougher sample paths (see Figure 5). With $\gamma = 0.5$, we have the standard Brownian motion. From Figure 5, we notice $f(0) = 0$ for all paths, which may be undesirable for the problems we consider in the paper. To avoid this, a fBM kernel can be centred.

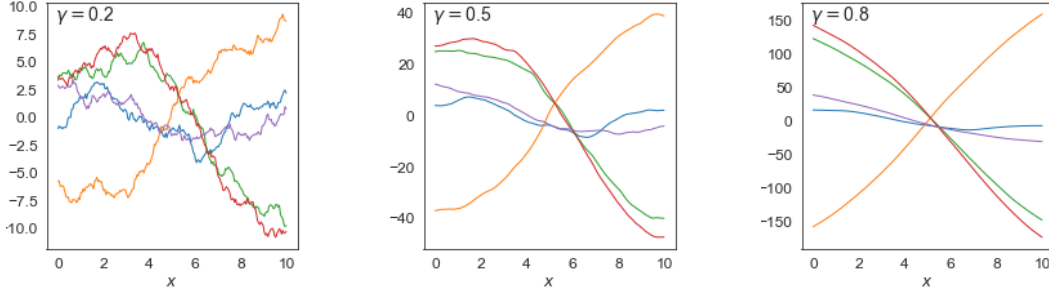


Fig 6: Sample paths ($y = f(x)$) from centred and squared fBM kernels constructed using (2.12) and (2.13) with different values for Hurst coefficient γ .

EXAMPLE 4 (centred fractional Brownian Motion kernel). Applying (2.10) to the fBM kernel (2.11), we have

$$k_{fbm_\gamma}^{(c)}(\mathbf{x}, \mathbf{x}') = \frac{\alpha^2}{2n^2} \sum_{i=1}^n \sum_{j=1}^n (||\mathbf{x} - \mathbf{x}_i||^{2\gamma} + ||\mathbf{x}' - \mathbf{x}_j||^{2\gamma} - ||\mathbf{x} - \mathbf{x}'||^{2\gamma} - ||\mathbf{x}_i - \mathbf{x}_j||^{2\gamma}) \quad (2.12)$$

In this paper, we will always center fBM kernels with respect to the empirical distribution.

Another issues with the fBM kernel in (2.11) is its roughness. In contrast to a GP with SE kernel, fractional Brownian motion paths are differentiable nowhere, hence they may be too rough to be used in many examples. To remedy this, we introduce a squared kernel.

DEFINITION 6 (Squared kernel). Let \mathcal{X} be a non-empty set. Given a kernel $k : \mathcal{X} \times \mathcal{X} \rightarrow \mathbb{R}$ and data $\mathbf{x}_i \in \mathcal{X}$ for $i = 1, \dots, n$, squared kernel is a function $k_{sq} : \mathcal{X} \times \mathcal{X} \rightarrow \mathbb{R}$ given by

$$k_{sq}(\mathbf{x}, \mathbf{x}') = \sum_{i=1}^n k(\mathbf{x}, \mathbf{x}_i)k(\mathbf{x}', \mathbf{x}_i), \quad \mathbf{x}, \mathbf{x}' \in \mathcal{X}. \quad (2.13)$$

As this kernel consists of products and sums of kernels, it is a positive definite kernel. The corresponding Gram matrix is given by $\mathbf{K}_{sq} = \mathbf{K}\mathbf{K}$. If we use the empirically centred kernel, the resulting Gram matrix $\mathbf{K}_{sq}^{(c)} = \mathbf{K}^{(c)}\mathbf{K}^{(c)}$ is also empirically centred, as we have

$$\mathbf{K}_{sq}^{(c)}\mathbf{1} = \mathbf{K}^{(c)}\left(\mathbf{K}^{(c)}\mathbf{1}\right) = \mathbf{K}^{(c)}\mathbf{0} = \mathbf{0}.$$

This kernel is shown useful in the previous work by Bergsma (2020); Jamil (2018); Jamil and Bergsma (2020) in the context of iprior, which has a close connection to GP regression and kernel methods. As shown in Figure 6, GP paths with squared (and centred) γ -fBM kernels are much smoother. In fact, the smoothness properties of GP paths with fBM kernel and squared fBM kernel can be discussed in terms of Hölder condition. While the realisations from the former are known to be a.s. Hölder of any order less than γ (see Embrechts and Maejima (2002) for example), the latter is Hölder of order 2γ . Bergsma (2020) discusses the smoothness properties of fBM paths and squared fBM path using different concepts of smoothness, including Hölder condition and regularity.

2.4. Estimation and inference. Let us revisit the regression model in (2.1) where we assume a zero-mean GP prior on f and i.i.d error. With $\mathbf{y} = (y_1, \dots, y_n)^\top$ and \mathbf{X} being a data matrix gathering covariates from all observations, we have:

$$\mathbf{y}|\mathbf{X} \sim \text{MVN}_n(\mathbf{0}, \mathbf{K} + \sigma^2\mathbf{I}). \quad (2.14)$$

The following sections discuss the posterior distribution and the estimation of the hyper-parameters.

2.4.1. *Posterior.* For Gaussian likelihood, GP is a conjugate prior, i.e., the posterior is also a GP. Specifically, we have $f|\mathbf{y}, \mathbf{X} \sim \text{GP}(\bar{m}, \bar{k})$ with the mean function $\bar{m} : \mathcal{X} \rightarrow \mathbb{R}$ and the kernel $\bar{k} : \mathcal{X} \times \mathcal{X} \rightarrow \mathbb{R}$ given by

$$\bar{m}(\mathbf{x}) = \mathbf{k}(\mathbf{x})^\top (\mathbf{K} + \sigma^2 \mathbf{I})^{-1} \mathbf{y}, \quad \mathbf{x} \in \mathcal{X} \quad (2.15)$$

$$\bar{k}(\mathbf{x}, \mathbf{x}') = k(\mathbf{x}, \mathbf{x}') - \mathbf{k}(\mathbf{x})^\top (\mathbf{K} + \sigma^2 \mathbf{I})^{-1} \mathbf{k}(\mathbf{x}'), \quad \mathbf{x}, \mathbf{x}' \in \mathcal{X} \quad (2.16)$$

where $\mathbf{k}(\mathbf{x}) = (k(\mathbf{x}_1, \mathbf{x}), \dots, k(\mathbf{x}_n, \mathbf{x}))^\top$ for $\mathbf{x} \in \mathcal{X}$. See Appendix A.1 for the derivation. The posterior given by (2.15) and (2.16) may more commonly be discussed in connection to prediction problems. In fact, given a new point \mathbf{x}^* the posterior predictive distribution over $f(\mathbf{x}^*)$ is Gaussian with mean $\bar{m}(\mathbf{x}^*)$ and variance $\bar{k}(\mathbf{x}^*, \mathbf{x}^*)$.

2.4.2. *Decomposition of the posterior under additive models and interpretability.* When the kernel and the regression function have an additive structure, i.e., $k_{all} = \sum_{j=1}^J k_j$ and $f_{all} = \sum_{j=1}^J f_j$ where each k_j is defined on $\mathcal{D}_j \times \mathcal{D}_j$ with a nonempty set \mathcal{D}_j and $f_j \sim \text{GP}(0, k_j)$, the posterior mean and kernel for the j -th term f_j can also be decomposed as

$$\bar{m}_j(\mathbf{x}_j) = \mathbf{k}_j(\mathbf{x}_j)^\top (\mathbf{K}_{all} + \sigma^2 \mathbf{I}_n)^{-1} \mathbf{y}, \quad \mathbf{x}_j \in \mathcal{D}_j \quad (2.17)$$

$$\bar{k}_j(\mathbf{x}_j, \mathbf{x}'_j) = \bar{k}_j(\mathbf{x}_j, \mathbf{x}'_j) - \mathbf{k}_j(\mathbf{x}_j)^\top (\mathbf{K}_{all} + \sigma^2 \mathbf{I}_n)^{-1} \mathbf{k}_j(\mathbf{x}'_j), \quad \mathbf{x}_j, \mathbf{x}'_j \in \mathcal{D}_j \quad (2.18)$$

for $j = 1, 2, \dots, J$ and J denoting the number of terms. Note that here we treat any tensor product kernel as one kernel, e.g. the j -th term can be $k_j(\mathbf{x}_j, \mathbf{x}'_j) = k_l(\mathbf{x}_l, \mathbf{x}'_l) k_{l'}(\mathbf{x}_{l'}, \mathbf{x}'_{l'})$ with $\mathbf{x}_j = (\mathbf{x}_l, \mathbf{x}_{l'})^\top$, $\mathbf{x}_l \in \mathcal{X}_l$, $\mathbf{x}_{l'} \in \mathcal{X}_{l'}$ and $\mathcal{D}_j = \mathcal{X}_l \times \mathcal{X}_{l'}$. As discussed in Plate (1999) and Duvenaud, Nickisch and Rasmussen (2011), one effective way to interpret an additive GP model is to visualise each function contributing to the model. If a kernel k_j is centred, the corresponding posterior mean function sums to zero over each input, i.e., $\sum_{i=1}^n \bar{m}_j(\mathbf{x}_{j,i}) = 0$. Furthermore, if we denote the posterior mean of the interaction effect term between \mathbf{x}_l and $\mathbf{x}_{l'}$ by $\bar{m}_{ll'}(\mathbf{x}_l, \mathbf{x}_{l'})$ and use centred k_l and $k_{l'}$, we have $\sum_{i=1}^n \bar{m}_{ll'}(\mathbf{x}_{li}, \mathbf{x}_{l'i}) = \sum_{i=1}^n \bar{m}_{ll'}(\mathbf{x}_l, \mathbf{x}_{l'i})$ for $\mathbf{x}_l \in \mathcal{X}_l$ and $\mathbf{x}_{l'} \in \mathcal{X}_{l'}$. This indicates that all terms in additive regression function, including main effects and lower-order interaction effects have intuitive interpretation and can be understood as averaged effects. See Appendix A.2 for further explanation and Section 4 for illustration with real-world data.

2.4.3. *Hyper-parameter estimation and model comparison.* The fully Bayesian way to estimate hyper-parameters, including parameters in the kernels and the variance in the error term σ^2 , is to put priors on them. In such case we most typically resort to Markov chain Monte Carlo (MCMC) to obtain samples from the posterior. Alternatively, we can use Empirical Bayes, where the parameters are estimated by maximising the log marginal likelihood denoted by $p(\mathbf{y}|\mathbf{X}) = \int p(\mathbf{y}|\mathbf{f})p(\mathbf{f}|\mathbf{X}, \mathbf{y})$. With Gaussian likelihood, this equals

$$\log p(\mathbf{y}|\mathbf{X}) = -\frac{1}{2} \mathbf{y}^\top (\mathbf{K} + \sigma^2 \mathbf{I}_n)^{-1} \mathbf{y} - \frac{1}{2} \log |\mathbf{K} + \sigma^2 \mathbf{I}_n| - \frac{n}{2} \log 2\pi. \quad (2.19)$$

Since more complex model does not necessarily lead to larger marginal likelihood (MacKay, 1995; Murray and Ghahramani, 2005), it can be used for comparing different models.

3. Efficient computation using Kronecker methods. The evaluation of the log marginal likelihood (2.19), the posterior mean (2.15) and covariance (2.16) involves the $n \times n$ marginal covariance matrix $\mathbf{K} + \sigma^2 \mathbf{I}$, and has a computational time complexity of $O(n^3)$ and storage requirements of $O(n^2)$. When a multidimensional grid structure is present in the data, these computations can be made efficient using Kronecker methods. More specifically, we focus on the data where the inputs form *Cartesian grid*, $\mathcal{X} = \mathcal{X}_1 \times \mathcal{X}_2 \times \dots \times \mathcal{X}_d$, where \mathcal{X}_l represents a set of observed values for the input dimension l and \times is the Cartesian product. With the example in Figure 1a, we have two dimensional grid structure with $\mathcal{X} = \mathcal{X}_1 \times \mathcal{X}_2$ where \mathcal{X}_1 and \mathcal{X}_2 are a set of geographical coordinates for all monitoring stations and a set of timestamps of each measurement. We let n_l represent the cardinality of set \mathcal{X}_l , i.e., $n_l = |\mathcal{X}_l|$. The total number of observations is therefore $n = \prod_{l=1}^d n_l$.

The primary component of this scalable method is a Kronecker product structure in a Gram matrix. See Section 3.1 of the Supplementary Material (Ishida and Bergsma, 2023) for introduction to the Kronecker product and its properties. If the two predictors form a two-dimensional grid, we can rewrite the model equation (2.1) as

$$y_{i,j} = f(\mathbf{x}_{1i}, \mathbf{x}_{2j}) + \epsilon_{i,j} \quad (3.1)$$

where $y_{i,j}$ is the response from the i, j -th location of the grid with $i = 1, \dots, n_1, j = 1, \dots, n_2$ and $n = n_1 n_2$. We write $\mathbf{y} = (y_{1,1}, \dots, y_{1,n_2}, \dots, y_{n_1,1}, \dots, y_{n_1,n_2})$ and define $\boldsymbol{\epsilon}$ similarly. The main effect and interaction effect models in (2.2) and (2.3) then can be specified by

$$f(\mathbf{x}_{1i}, \mathbf{x}_{2j}) = a + f_1(\mathbf{x}_{1i}) + f_2(\mathbf{x}_{2j}) \quad (3.2)$$

$$f(\mathbf{x}_{1i}, \mathbf{x}_{2j}) = a + f_1(\mathbf{x}_{1i}) + f_2(\mathbf{x}_{2j}) + f_{12}(\mathbf{x}_{1i}, \mathbf{x}_{2j}). \quad (3.3)$$

If we use the same prior as the previous model with $\alpha_0 = 1$, we have $\mathbf{y}|\mathbf{X} \sim \text{MVN}_n(\mathbf{0}, \mathbf{K} + \sigma^2 \mathbf{I}_n)$ with the Gram matrix for each model given by

$$\mathbf{K} = \mathbf{1}_{n_1} \mathbf{1}_{n_1}^\top \otimes \mathbf{1}_{n_2} \mathbf{1}_{n_2}^\top + \mathbf{K}_1 \otimes \mathbf{1}_{n_2} \mathbf{1}_{n_2}^\top + \mathbf{1}_{n_1} \mathbf{1}_{n_1}^\top \otimes \mathbf{K}_2. \quad (3.4)$$

$$\mathbf{K} = (\mathbf{1}_{n_1} \mathbf{1}_{n_1}^\top + \mathbf{K}_1) \otimes (\mathbf{1}_{n_2} \mathbf{1}_{n_2}^\top + \mathbf{K}_2)$$

where \otimes is a Kronecker product operator. We relax the assumption on α_0 later in section 3.3. In what follows, we show that how we can exploit these structured Gram matrix for efficient computation. In Section 3.1, we outline the general procedures of the Kronecker approach, with the key operation being the eigendecomposition of the Gram matrix. We illustrate how this can be achieved for models employing saturated and non-saturated hierarchical ANOVA kernels in Sections 3.2 and 3.3, respectively.

3.1. General procedure of Kronecker approach. For Kronecker product involving d matrices, we write $\bigotimes_{l=1}^d \mathbf{A}_l = \mathbf{A}_1 \otimes \mathbf{A}_2 \otimes \dots \otimes \mathbf{A}_d$. For d dimensional grid data, the main idea of Kronecker methods is to decompose the Gram matrix in the form:

$$\mathbf{K} = \left(\bigotimes_{l=1}^d \mathbf{Q}_l \right) \mathbf{D} \left(\bigotimes_{l=1}^d \mathbf{Q}_l \right)^\top \quad (3.5)$$

where each \mathbf{Q}_l , and hence also $\mathbf{Q} := \bigotimes_{l=1}^d \mathbf{Q}_l$, is orthonormal and \mathbf{D} is diagonal with non-negative entries. Once we obtain this decomposition, the log determinant of the marginal covariance matrix can be computed by

$$\log |\mathbf{K} + \sigma^2 \mathbf{I}| = \sum_{i=1}^n \log(\mathbf{D}_{i,i} + \sigma^2)$$

where $\mathbf{D}_{i,i}$ is the i -th diagonal element of \mathbf{D} . This costs $O(n)$ operations. The multiplication of the inverted matrix and a vector \mathbf{v} can be expressed as

$$(\mathbf{K} + \sigma^2 \mathbf{I}_n)^{-1} \mathbf{v} = \left(\bigotimes_{l=1}^d \mathbf{Q}_l \right) (\mathbf{D} + \sigma^2 \mathbf{I}_n)^{-1} \left(\bigotimes_{l=1}^d \mathbf{Q}_l \right)^\top \mathbf{v}. \quad (3.6)$$

The inversion of the middle diagonal matrix can be done by simply inverting its diagonal elements. Evaluating the above also requires matrix-vector multiplication $(\bigotimes_{l=1}^d \mathbf{Q}_l)^\top \mathbf{v}$. Let us rewrite this expression by

$$\left(\bigotimes_{l=1}^d \mathbf{Q}_l \right)^\top \mathbf{v} = \left(\bigotimes_{l=1}^d \mathbf{Q}_l^\top \right) \mathbf{v} = \left(\bigotimes_{l=1}^{d-1} \mathbf{Q}_l^\top \right) \mathbf{v}_d \quad (3.7)$$

where $\mathbf{v}_d = \text{vec}(\mathbf{Q}_d^\top \mathbf{V})$ with $\text{vec}(\mathbf{A})$ being a vectorisation operator transforming a $p \times q$ matrix \mathbf{A} to a vector of length pq by stacking the columns of the matrix, and \mathbf{V} is a $n_d \times \frac{n}{n_d}$ matrix whose elements are filled with elements of vector \mathbf{v} in column-major order. Computing \mathbf{v}_d takes $O(n_l^2 \frac{n}{n_l}) = O(nn_l)$. Iteratively applying this to get $\mathbf{v}_{d-1} = \text{vec}(\mathbf{Q}_{d-1}^\top \mathbf{V}_d)$, $\mathbf{v}_{d-2} = \text{vec}(\mathbf{Q}_{d-2}^\top \mathbf{V}_{d-1})$, \dots , $\mathbf{v}_1 = \text{vec}(\mathbf{Q}_1^\top \mathbf{V}_2)$ thus requires $O(n \sum_{l=1}^d n_l)$ operations, and the final vector \mathbf{v}_1 equals $(\bigotimes_{l=1}^d \mathbf{Q}_l)^\top \mathbf{v}$. The complete algorithm is described in [Saatçi \(2012, Chapter 5\)](#) and [Wilson et al. \(2014\)](#).

The Kronecker method has been used and proven useful for efficient implementation of GP models (e.g. [Saatçi \(2012, Chapter 5\)](#), [Groot et al. \(2014\)](#) [Wilson et al. \(2014\)](#) and [Flaxman et al. \(2015\)](#)). However, the existing method is applicable to limited sub-models with so-called separable kernel structures. This includes models with tensor-product kernel or saturated ANOVA decomposition kernel and is not capable of handling the non-saturated models that involve addition of matrices in a Kronecker product form, such as (3.4). As mentioned previously using a tensor product kernel implies including only the interaction term of the highest order. This may be problematic in many applications where assessing the effect of each predictor is needed. On the other hand, using the saturated ANOVA kernel means that we assume a saturated model, which could often overfit the data.

3.2. Gram matrix decomposition for saturated ANOVA kernel. Now let us assume that we have d -dimensional grid structure in the predictors. We have a response vector \mathbf{y} of length n . If we use the saturated ANOVA decomposition kernel (2.8), the Gram matrix can be written as

$$\mathbf{K} = \bigotimes_{l=1}^d \tilde{\mathbf{K}}_l$$

where $\tilde{\mathbf{K}}_l = (\mathbf{1}_n \mathbf{1}_{n_l}^\top + \mathbf{K}_l)$ and $\mathbf{K}_l = \{k_{l,(i,j)}\}_{n_l \times n_l}$ with $k_{l,(i,j)} = k_l(\mathbf{x}_{l,i}, \mathbf{x}_{l,j})$. Using the eigendecomposition, $\tilde{\mathbf{K}}_l = \tilde{\mathbf{Q}}_l \tilde{\Lambda}_l \tilde{\mathbf{Q}}_l^\top$ and the mixed product properties (see Section 3.1 and 3.2 of the Supplementary Material ([Ishida and Bergsma, 2023](#))), we can write

$$\mathbf{K} = \left(\bigotimes_{l=1}^d \tilde{\mathbf{Q}}_l \right) \left(\bigotimes_{l=1}^d \tilde{\Lambda}_l \right) \left(\bigotimes_{l=1}^d \tilde{\mathbf{Q}}_l \right)^\top. \quad (3.8)$$

Note that $\tilde{\mathbf{Q}} := \left(\bigotimes_{l=1}^d \tilde{\mathbf{Q}}_l \right)$ is orthonormal and $\tilde{\Lambda} := \left(\bigotimes_{l=1}^d \tilde{\Lambda}_l \right)$ is diagonal with non-negative entries as each $\tilde{\mathbf{K}}_l$ is positive semi-definite.

3.3. *Gram matrix decomposition for nonsaturated hierarchical ANOVA kernel.* We now show that the Kronecker product structure can be exploited for efficient computation even when we have a more general structure in the kernel, such as (3.4), by using an empirically centred kernel (2.10). Consider a hierarchical ANOVA kernel for data with a d -dimensional grid structure. Let us now assume that we have m terms in our additive kernel where $1 + d \leq m \leq 2^d$. The corresponding Gram matrix \mathbf{K} then also involves addition of m matrices \mathbf{M}_p for $p = 1, \dots, m$:

$$\mathbf{K} = \sum_{p=1}^m \mathbf{M}_p \quad (3.9)$$

where

$$\mathbf{M}_p = \bigotimes_{l=1}^d \mathbf{B}_l \quad \text{where} \quad \mathbf{B}_l = \begin{cases} \mathbf{K}_l^{(c)}, & \text{if } k_l^{(c)} \text{ is involved in the } p\text{-th term} \\ \mathbf{1}_{n_l} \mathbf{1}_{n_l}^\top, & \text{otherwise.} \end{cases}$$

For this class of Gram matrices, we have the following lemma.

LEMMA 1. *A matrix \mathbf{K} of the form given by (3.9) has the following decomposition:*

$$\mathbf{K} = \left(\bigotimes_{l=1}^d \mathbf{Q}_l^{(c)} \right) \mathbf{D} \left(\bigotimes_{l=1}^d \mathbf{Q}_l^{(c)} \right)^\top$$

where $\mathbf{Q}_l^{(c)}$ is orthonormal matrix whose columns consist of eigenvectors of $\mathbf{K}_l^{(c)}$, and \mathbf{D} is diagonal with non-negative entries.

PROOF. From Lemma 3 (see A.3 and A.6), for $l = 1, \dots, d$, we have:

$$\begin{aligned} \mathbf{K}_l^{(c)} &= \mathbf{Q}_l^{(c)} \mathbf{\Lambda}_l^{(c)} \mathbf{Q}_l^{(c)\top} \\ \mathbf{1}_{n_l} \mathbf{1}_{n_l}^\top &= \mathbf{Q}_l^{(c)} \mathbf{A}_l \mathbf{Q}_l^{(c)\top} \end{aligned} \quad (3.10)$$

where (3.10) is an eigendecomposition of a centred matrix $\mathbf{K}_l^{(c)}$ i.e., $\mathbf{Q}_l^{(c)}$ is orthonormal, $\mathbf{\Lambda}_l^{(c)}$ is diagonal with non-negative eigenvalues in the diagonal (see A.4 and A.5) and \mathbf{A}_l is a $n_l \times n_l$ matrix with $\mathbf{A}_{1,1} = n_l$ and 0 everywhere else. Then using the mixed product property of Kronecker products, we can decompose \mathbf{M}_p as

$$\mathbf{M}_p = \bigotimes_{l=1}^d \mathbf{Q}_l^{(c)} \bigotimes_{l=1}^d \mathbf{D}_{pl} \bigotimes_{l=1}^d \mathbf{Q}_l^{(c)\top}$$

where

$$\mathbf{D}_{pl} = \begin{cases} \mathbf{\Lambda}_l^{(c)} & \text{if } k_l^{(c)} \text{ is involved in the } p\text{-th term} \\ \mathbf{A}_l & \text{otherwise.} \end{cases}$$

Let $\mathbf{D}_p = \bigotimes_{l=1}^d \mathbf{D}_{pl}$. We have

$$\begin{aligned} \mathbf{K} &= \sum_{p=1}^m \mathbf{M}_p = \sum_{p=1}^m \left(\bigotimes_{l=1}^d \mathbf{Q}_l^{(c)} \mathbf{D}_p \bigotimes_{l=1}^d \mathbf{Q}_l^{(c)\top} \right) \\ &= \bigotimes_{l=1}^d \mathbf{Q}_l^{(c)} \left(\sum_{p=1}^m \mathbf{D}_p \right) \bigotimes_{l=1}^d \mathbf{Q}_l^{(c)\top}. \end{aligned} \quad (3.11)$$

It is easy to see that each \mathbf{D}_p and hence also the matrix $\mathbf{D} := \sum_{p=1}^m \mathbf{D}_p$ is diagonal with non-negative diagonal entries. \square

EXAMPLE 5 (Example of the Kronecker method for a hierarchical ANOVA kernel with $d = 2$). Consider a model specified by (3.1) and (3.2), i.e., the main effect model for two-dimensional grid data. If we use centred kernels, the Gram matrix given by (3.4) can be written as

$$\mathbf{K} = \mathbf{1}_{n_1} \mathbf{1}_{n_1}^\top \otimes \mathbf{1}_{n_2} \mathbf{1}_{n_2}^\top + \mathbf{K}_1^{(c)} \otimes \mathbf{1}_{n_2} \mathbf{1}_{n_2}^\top + \mathbf{1}_{n_1} \mathbf{1}_{n_1}^\top \otimes \mathbf{K}_2^{(c)}$$

and can be decomposed as

$$\begin{aligned} \mathbf{K} &= \mathbf{Q}_1^{(c)} \mathbf{A}_1 \mathbf{Q}_1^{(c)\top} \otimes \mathbf{Q}_2^{(c)} \mathbf{A}_2 \mathbf{Q}_2^{(c)\top} + \mathbf{Q}_1^{(c)} \mathbf{\Lambda}_1 \mathbf{Q}_1^{(c)\top} \otimes \mathbf{Q}_2^{(c)} \mathbf{A}_2 \mathbf{Q}_2^{(c)\top} \\ &\quad + \mathbf{Q}_1^{(c)} \mathbf{A}_1 \mathbf{Q}_1^{(c)\top} \otimes \mathbf{Q}_2^{(c)} \mathbf{\Lambda}_2 \mathbf{Q}_2^{(c)\top} \\ &= \left(\mathbf{Q}_1^{(c)} \otimes \mathbf{Q}_2^{(c)} \right) \left(\mathbf{A}_1 \otimes \mathbf{A}_2 + \mathbf{\Lambda}_1 \otimes \mathbf{A}_2 + \mathbf{A}_1 \otimes \mathbf{\Lambda}_2 \right) \left(\mathbf{Q}_1^{(c)} \otimes \mathbf{Q}_2^{(c)} \right)^\top. \end{aligned}$$

Thus far, we have restricted the prior variance of the constant term a in (3.2) and (3.3) to be 1. Lifting this assumption is straightforward. If the prior variance is α_0^2 , the decomposition of the corresponding Gram matrix can be expressed in the same way as (3.8) and (3.11) with all elements of the middle diagonal matrix multiplied by α_0^2 .

3.4. *Computational complexity and space requirement.* Kronecker methods significantly reduce the cost of computing the log determinant of the matrix $\mathbf{K} + \sigma^2 \mathbf{I}$, and solving the linear system $(\mathbf{K} + \sigma^2 \mathbf{I})^{-1} \mathbf{v}$, which usually has $O(n^3)$ when \mathbf{K} is an $n \times n$ Gram matrix. As seen in (3.1) and (3.7), the key operations are eigendecomposition to get eigenvalues and a matrix of eigenvectors, and matrix-vector multiplication involving Kronecker products. With a Kronecker product structure, eigendecomposition is applied to each \mathbf{K}_l of size $n_l \times n_l$ individually, which has $O(n_l^3)$ complexity. The total cost for the eigendecomposition of \mathbf{K} then reduces to $O(\sum_{l=1}^d n_l^3)$, which is dominated by the largest of n_l . The second component is a matrix-vector multiplication in $(\otimes_{l=1}^d \mathbf{Q}_l^\top) \mathbf{v}$. A matrix-vector multiplication of an $n \times n$ matrix and a vector of length n usually requires $O(n^2)$ operations. Using the algorithm provided in Saatçi (2012, Chapter 5) and Wilson et al. (2014), this Kronecker product matrix-vector multiplication takes $O(n \sum_{l=1}^d n_l)$ which is much less than the usual $O(n^2)$. Once we have eigenvalues of all sub-Gram matrices \mathbf{K}_l , computing the log-determinant has an additional cost of $O(n)$. The storage requirement reduces from $O(n^2)$ to $O(\sum_{l=1}^d n_l^2)$ which is associated with storing matrices $\mathbf{Q}_1, \dots, \mathbf{Q}_d$. Previous work by Saatçi (2012) and Wilson et al. (2014) explored the use of the Kronecker method in Gaussian process regression and demonstrated improved computational time through simulation studies. Our approach, which shares the same key factors determining computational cost (namely, eigendecomposition of Gram matrices and matrix-vector multiplication), is expected to yield similar computational gains.

3.5. *Other scalable approaches.* A number of methods have been proposed to enhance the scalability of Gaussian process models. As summarized by Liu et al. (2020), one mainstream approach involves approximating the Gram matrix \mathbf{K} . This can be achieved by utilizing a subset of data, typically of size $m \ll n$ (subset-of-data), or by exploiting sparsity in the Gram matrix. This is based on the assumption that the covariance between distant points is zero, resulting in sparse kernels (Melkumyan and Ramos, 2009). A particularly popular technique is the low-rank approximation using inducing points (e.g., Titsias (2009));

Hensman, Fusi and Lawrence (2013)), inspired by Nystrom’s method (Williams and Seeger, 2001). In spatio-temporal setting, Datta et al. (2016) introduced dynamic nearest neighbour GP that induces a sparse structure in the inverse of the covariance matrix with additive kernel structures. This was used to analyse air pollution data similar in size to the data in our study. Unlike the Kronecker approach, which necessitates a multi-dimensional grid structure for the data, these methods can be applied to broad data structure. However, the Kronecker approach offers the advantage of avoiding approximation, as it rather exploits the structure of the data to efficiently evaluate and store the key components required for estimation and inference. In fact, the Kronecker approach and other scalable methods can complement each other, as exemplified by Wilson and Nickisch (2015), who incorporated a grid structure into inducing points. Although their work focused on the tensor product kernel, the method can be extended to handle additive kernels using the decomposition discussed in Section 3.3.

4. Application to NO₂ concentration in London. We applied our method to analyse a dataset of hourly nitrogen dioxide (NO₂) concentrations in London covering the period before and after the first COVID-19 lockdown in the UK. NO₂ is a harmful air pollutant that adversely affects human health and the environment. Short-term exposure to high levels of NO₂ can irritate the respiratory system, exacerbating conditions like asthma, while prolonged exposure is linked to lung and cardiovascular diseases. Additionally, NO₂ contributes to environmental damage through acid rain, smog, and ozone formation. According to the World Health Organization, recommended ambient NO₂ concentration levels are below $10\mu\text{g}/\text{m}^3$ for the annual mean and at most 3-4 exceedance days per year with a 24-hour mean of $25\mu\text{g}/\text{m}^3$. Investigating the direct and indirect effects of policy interventions and regulation changes that reduce NO₂ emissions is crucial. One example of such indirect policy intervention is the lockdown measures taken across the world. In urban areas like London, vehicle emissions are the main source of NO₂. A number of studies have shown that restricted mobility due to the lockdown has contributed to a drop in NO₂ concentration in the air on a global scale (See Dutta, Kumar and Dubey (2021) and Cooper et al. (2022) for example). By examining measurement data from monitoring stations across the country, a comparable conclusion was drawn at the national level in the UK (Lee et al., 2020; Higham et al., 2021; Jephcote et al., 2021). The majority of such studies analyse the average daily concentrations. While daily mean data are suitable when the research question revolves around assessing long-term changes in the concentration level, interesting findings may be reached by analysing hourly-recorded data. It is known that the concentration of NO₂ in the air varies over the course of a day, with a distinct daily cycle. If we are to investigate the effect of lockdown, in addition to studying the average downtrend, which is typically done by analysing daily or weekly average data, one may ask if the daily cycle changed over time during this period. With measurement data from multiple sites, it is also possible to study spatial patterns, and with that pattern identified, we can conduct further research on spatio-temporal interaction. That is, we can let the daily cycle or global time trend be different at different locations. Answering these questions requires analysis of hourly-measured data over a number of days at different locations, which easily results in massive data. However such data typically have a balanced panel structure as described in the next section, and can be analysed efficiently using the proposed Kronecker approach. Although our data analysis is exploratory, we aim to show that flexible additive Gaussian process models combined with this Kronecker method make it possible to investigate important research questions that would have been otherwise infeasible.

4.1. *Dataset.* we used a dataset of NO₂ concentrations (measured in $\mu\text{g}/\text{m}^3$) collected at various sites in the London Air Quality network¹ during the period from January 6th, 2020

¹<https://www.londonair.org.uk>

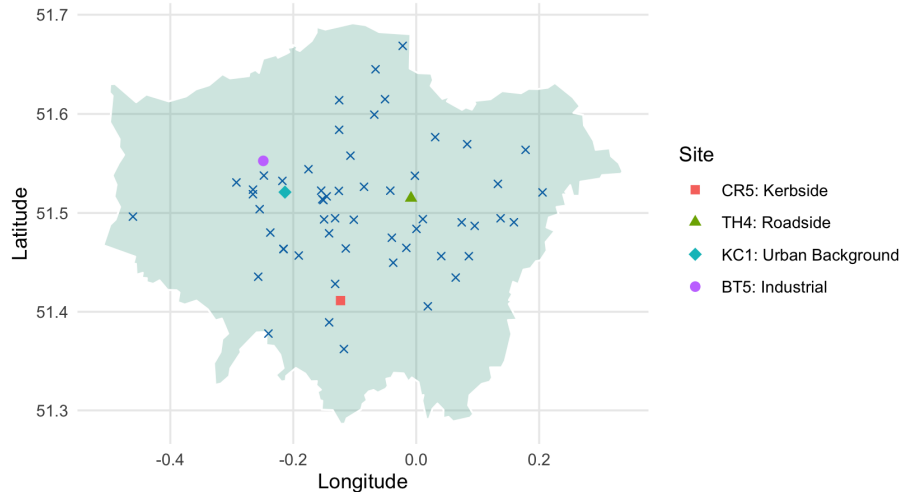


Fig 7: The location of NO₂ measurement sites included in the dataset. Four sites are selected and labelled for illustration purposes. Site CR5 is in the Borough of Croydon, while TH4, KC1 and BT5 are in Tower Hamlets, Kensington and Chelsea, and Brent. The sites in the dataset are classified into 5 categories: Kerbside, Roadside, Urban Background, Suburban and Industrial.

to May 30th, 2020. We excluded sites with more than 30% missing values or more than 48 consecutive missing values, resulting in a total of 59 sites and 208,152 observations. As seen in Figure 2, the data has a three-level structure: site location (Easting and Northing), day, and hour of the day. To accommodate the Kronecker method, which usually requires a complete grid structure, we imputed the remaining missing values following the steps outlined in Appendix B.1. Although the method used for imputation is simple, due to a very small proportion (0.62%) of missing values, we believe that any bias introduced does not have significant impact. Another issue to consider is the transformation of the response, NO₂ concentrations. While they are typically modeled on a log-scale to address the right skewness commonly found in air pollutant concentration data, due to the presence of zero and negative records (accounting for measurement equipment uncertainty), we retained the response variable in its original scale. The observed NO₂ levels range from -2.9 to 320.6 . Additionally, we adjusted for the transition from winter time to summer time during the study period (details provided in Appendix B.1).

4.2. *Model formulation.* As shown in Figure 2, the dataset has a three-dimensional grid structure, with location, day and hour as predictors, denoted by $\mathbf{x}_1 \in \mathcal{X}_1$, $x_2 \in \mathcal{X}_2$ and $x_3 \in \mathcal{X}_3$ where $\mathcal{X}_1 \subset \mathbb{R}^2$, \mathcal{X}_2 represents the set of calendar dates numbered $1, 2, \dots$, and \mathcal{X}_3 represent hour of the day indexed by $1, 2, \dots, 24$. Let $y_{s,d,h}$ denote the observed NO₂ concentration from monitoring station s , on day d at hour h where $s = 1, \dots, n_1$, $d = 1, \dots, n_2$, $h = 1, \dots, n_3$ and $n_1 = 59$, $n_2 = 147$, $n_3 = 24$. To model the response, we consider a function of three variables $f : \mathcal{X} = \mathcal{X}_1 \times \mathcal{X}_2 \times \mathcal{X}_3 \rightarrow \mathbb{R}$ and assume a zero mean GP prior. Revising the model in 2.1, we have

$$y_{s,d,h} = f(\mathbf{x}_{1s}, x_{2d}, x_{3h}) + \epsilon_{s,d,h}$$

with $f \sim \text{GP}(0, k)$ where a covariance kernel $k : \mathcal{X} \times \mathcal{X} \rightarrow \mathbb{R}$ is modelled according to our prior belief. We assume i.i.d error with $\epsilon_{s,d,h} \sim N(0, \sigma^2)$. We consider several kernels that belong to a class of hierarchical ANOVA decomposition kernels and the tensor product

kernel. Note that for $l = 1, 2, 3$, we denote the base kernel for each predictor by k_l defined on $\mathcal{X}_l \times \mathcal{X}_l$ and assume $f_l \sim \text{GP}(0, k_l)$. The interaction terms are constructed using the tensor product kernel (2.6). For the model specification, we drop the subscripts s, d, h to simplify the expression.

4.2.1. *List of models.* We list the kernels for the models we consider for this dataset. Note that the prior over the overall function f follows zero mean GP with kernel $k = \alpha_0^2 k_{m_j}$ for $j = 1, \dots, 5$.

Model 1: main effect

The first model we consider is the main effect model, where $f(\mathbf{x}_1, x_2, x_3)$ and the kernel are given by

$$\begin{aligned} f(\mathbf{x}_1, x_2, x_3) &= a + f_1(\mathbf{x}_1) + f_2(x_2) + f_3(x_3) \\ k_{m1} &= 1 + k_1 + k_2 + k_3. \end{aligned}$$

The Gram matrix with this kernel and all other kernels under consideration are given in Appendix B.2. This model does not involve any interaction effects, meaning that the effect of the location is constant throughout the whole period. Or equivalently, the global time trend captured using the day predictor x_2 and the daily cyclical effect captured by the hour predictor x_3 are both assumed the same for all sites. We use Model 1 as the baseline model and extend it to include two-way or three-way interaction effects.

Model 2: space-time interaction

If we assume a space and time interaction, i.e., both the global time trend and the daily cycle are different at different location, we have Model 2 specified by

$$\begin{aligned} f(\mathbf{x}_1, x_2, x_3) &= a + f_1(\mathbf{x}_1) + f_2(x_2) + f_3(x_3) + f_{12}(\mathbf{x}_1, x_2) + f_{13}(\mathbf{x}_1, x_2) \\ k_{m2} &= k_{m1} + k_1 \otimes k_2 + k_1 \otimes k_3. \end{aligned}$$

Model 3: all two-way interaction

The model with all two-way interactions extends Model 2 by

$$\begin{aligned} f(\mathbf{x}_1, x_2, x_3) &= a + f_1(\mathbf{x}_1) + f_2(x_2) + f_3(x_3) + f_{12}(\mathbf{x}_1, x_2) + f_{13}(\mathbf{x}_1, x_2) + f_{23}(x_2, x_3) \\ k_{m3} &= k_{m2} + k_2 \otimes k_3 \end{aligned}$$

and adds further assumption that the daily cycle changes over time.

Model 4: saturated/three-way interaction model

If we consider the saturated model with a three-way interaction, the model equals

$$\begin{aligned} f(\mathbf{x}_1, x_2, x_3) &= a + f_1(\mathbf{x}_1) + f_2(x_2) + f_3(x_3) + \\ &f_{12}(\mathbf{x}_1, x_2) + f_{13}(\mathbf{x}_1, x_2) + f_{23}(x_2, x_3) + f_{123}(\mathbf{x}_1, x_2, x_3) \\ k_{m4} &= k_{m3} + k_1 \otimes k_2 \otimes k_3. \end{aligned}$$

Note that this is the saturated ANOVA decomposition kernel for three-dimensional grid data.

Model 5: three-way interaction only

Finally, we also fit a model with only the three-way interaction term, of which the model function f and the kernel are given by

$$\begin{aligned} f(\mathbf{x}_1, x_2, x_3) &= f_{123}(\mathbf{x}_1, x_2, x_3) \\ k_{m5} &= k_1 \otimes k_2 \otimes k_3. \end{aligned}$$

Although this separable kernel is widely used in machine learning applications, with this kernel construction, the interpretation of the effects of each predictor is difficult. The result shows that it fits the data poorly compared to other models under consideration.

TABLE 1

Results from fitting Model 1 to Model 5 to London NO_2 data. The difference of the log marginal likelihood in comparison to that of the baseline model (Model 1) is shown as $\Delta\text{mloglik}$. The log marginal likelihood for Model 1 is -857,889. The average time (in minutes) taken to obtain 2 chains of 300 MCMC samples after the 200 warm-up phase is also displayed. For model 5, we only need one scale parameter α_1 due to identifiability issues.

Model	α_0	α_1	α_2	α_3	σ	$\Delta\text{mloglik}$	Time
1: main	6.865	5.076	2.228	0.335	14.850	-	20.9
2: spatio-temporal interaction	14.363	1.288	0.674	0.236	12.535	25,834	14.3
3: all two-way interaction	10.669	1.862	1.321	0.306	8.367	98,070	17.5
4: saturated	52.050	0.482	0.941	0.0512	6.508	104,109	17.1
5: three-way interaction only	-	0.0008052	-	-	36.4303	-186,450	1.96

4.2.2. *Kernel choice.* The choice of baseline kernels k_l is also an important factor that reflects our prior belief about the underlying process. As discussed in Section 2.3, a GP with the squared-centred standard Brownian motion kernel ($\gamma = 0.5$) has good smoothness properties. This kernel, as well as other fractional Brownian motion-based kernels, has a computational advantage over other common kernels such as squared exponential kernels, as we do not have to perform eigendecomposition or matrix-vector multiplication at each iteration of a chosen optimisation algorithm (See Section 3.2.1 of the Supplementary material (Ishida and Bergsma, 2023)). We use this as a starting point and explore different options. We found that the spatial process f_1 is rougher than the temporal processes f_2, f_3 . To determine the optimal values for the Hurst coefficient γ in k_1 , we conducted a grid search, which led to the choice of $\gamma = 0.3$. For k_2 and k_3 , squared-centred standard Brownian motion kernels ($\gamma = 0.5$) produced a good fit. We put priors on the rest of the hyper-parameters, including the scale parameters of overall kernel and each base kernels, $\alpha_0, \alpha_1, \alpha_2, \alpha_3$, and the variance of the error term σ^2 and estimated them by the posterior mean from MCMC samples. The specified models are implemented using the programming language Stan. The code is provided in the Supplementary Material. The online version is available at github.com/sahokoishida/Additive-GP-Kronecker.

4.3. *Results.* The main results are shown in Table 1, including the point estimates of hyper-parameters, log marginal likelihood improvement compared to the baseline model and computational time. From the log marginal likelihood values for Model 1 to Model 4, we see that the fit to the data improves as the model becomes more complex. It is apparent that Model 3 (all two-way interactions) offers significant improvement compared to Models 2 (spatio-temporal interaction), indicating the importance of including the additional interaction term between daily cycle and global time effect. The improvement in the log-marginal likelihood by including the three-way interaction is not as large, however, as we still see a major improvement, we conclude that Model 4 (saturated) is the best model. It is important to note, however, the saturated model does not always offer the best fit, and in order to confirm the presence of higher order interactions, a comparison to simpler models is essential. MCMC sampling took less than 20 minutes on average for all models. Note that Model 5, which took 1.96 minutes, only has two model parameters. We also estimated hyper-parameters by finding maximiser of the log marginal likelihood (2.19), which took a few seconds for each model as shown in Appendix B.3. It can also be seen that the interaction-only model performs worse than the simple main effect model. In Figure 8, we show the posterior mean and the 2.5% and 97.5% quantiles of the posterior predictive distribution derived by Model 3, at selected sites (see Table 7) from the 23rd of March for two weeks together with the corresponding observed values. We see that the posterior predictive mean captures the overall trend well, but smoother than the observed. The model comparison implies that, on top of the space-time interaction, the effect of the hours of the day interacts with the effects of global time. That is,

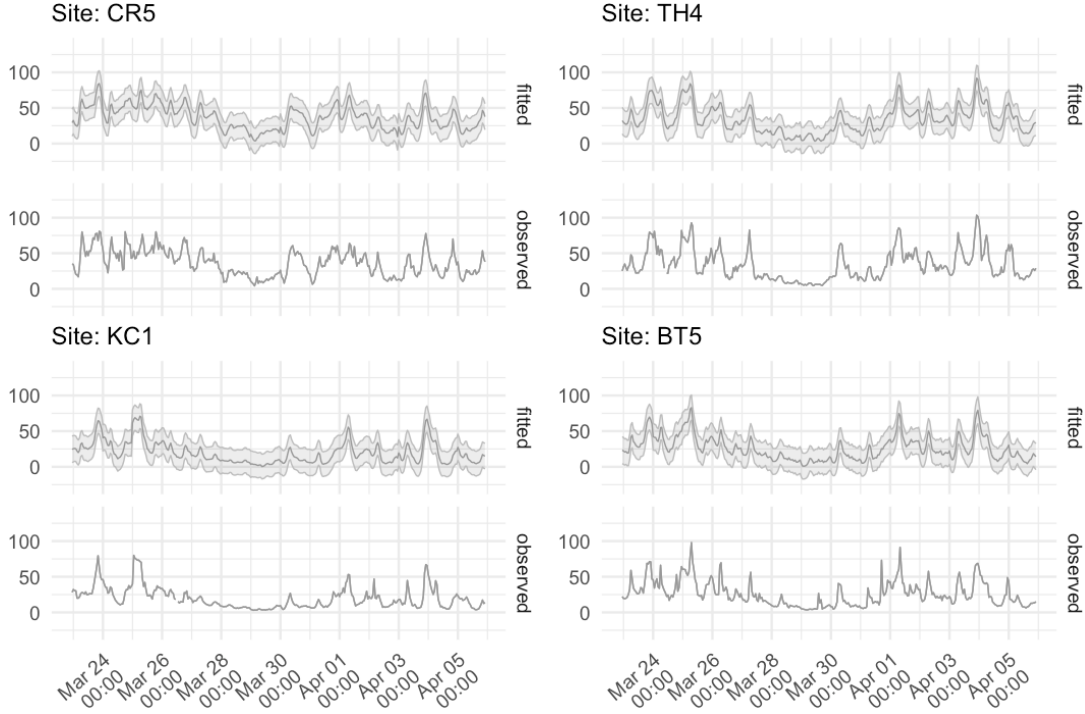


Fig 8: Observed and fitted (with 95% predictive bands) NO₂ concentrations (in $\mu\text{g}/\text{m}^3$) at 4 different sites

the global time trend and the daily cycle of NO₂ concentration level are different for different locations, and the identified daily cycle also changes over time. Furthermore, the fact that the additional three-way interaction term led to further improvement in log marginal likelihood suggests that this change in daily pattern over time depends on the measurement sites.

4.4. *Visualisation and interpretation of each effect.* To interpret the chosen model (Model 4), we can visualise each effect using the mean decomposition of additive GP models seen in (2.17). We denote the posterior mean function of the main effect terms by \bar{m}_l for $l = 1, 2, 3$, two-way interaction effect terms by $\bar{m}_{ll'}$ for $1 \leq l < l' \leq 3$, and the three-way interaction effect term by \bar{m}_{123} . In addition, we have the mean of the constant term $\bar{m}_a = 28.988$. As discussed in Section 2.4.2, due to centering of kernels, the mean of the main effect, as well as mean (over each covariate) of interaction effect is zero, e.g., we have $\sum_{s=1}^{59} \bar{m}_1(\mathbf{x}_{1,s}) = 0$, $\sum_{d=1}^{147} \bar{m}_{23}(x_{2,d}, x_{3,h}) = 0$ and $\sum_{h=1}^{24} \bar{m}_{123}(\mathbf{x}_{1,s}, x_{2,d}, x_{3,h}) = 0$. This allow for interpreting the lower order interaction effects, including the main effects, as averaged effects. In what follows, we visualise and interpret the main effects, selected two-way interaction effects and the three-way interaction effects.

Figure 9 shows the three main effects $\bar{m}_1(\mathbf{x}_1)$, $\bar{m}_2(x_2)$ and $\bar{m}_3(x_3)$. From Figure 9a showing spatial effect averaged over hour of the day and calendar date, we see a few hot spots in central London, and a negative effect in outskirts of London especially towards the east. However, as we did not take into account the types of the sites in modelling, we need to be careful with the interpretation. The average global time effect is visualised in Figure 9c. We notice a small downward trend over the period. Whether this is the effect of the lockdown or the result of lower emission from e.g. heating source due to warmer weather needs further investigation. For example, we can compare the records from previous years, or incorporate information such as temperature in the model. Short-term variation is also apparent. There

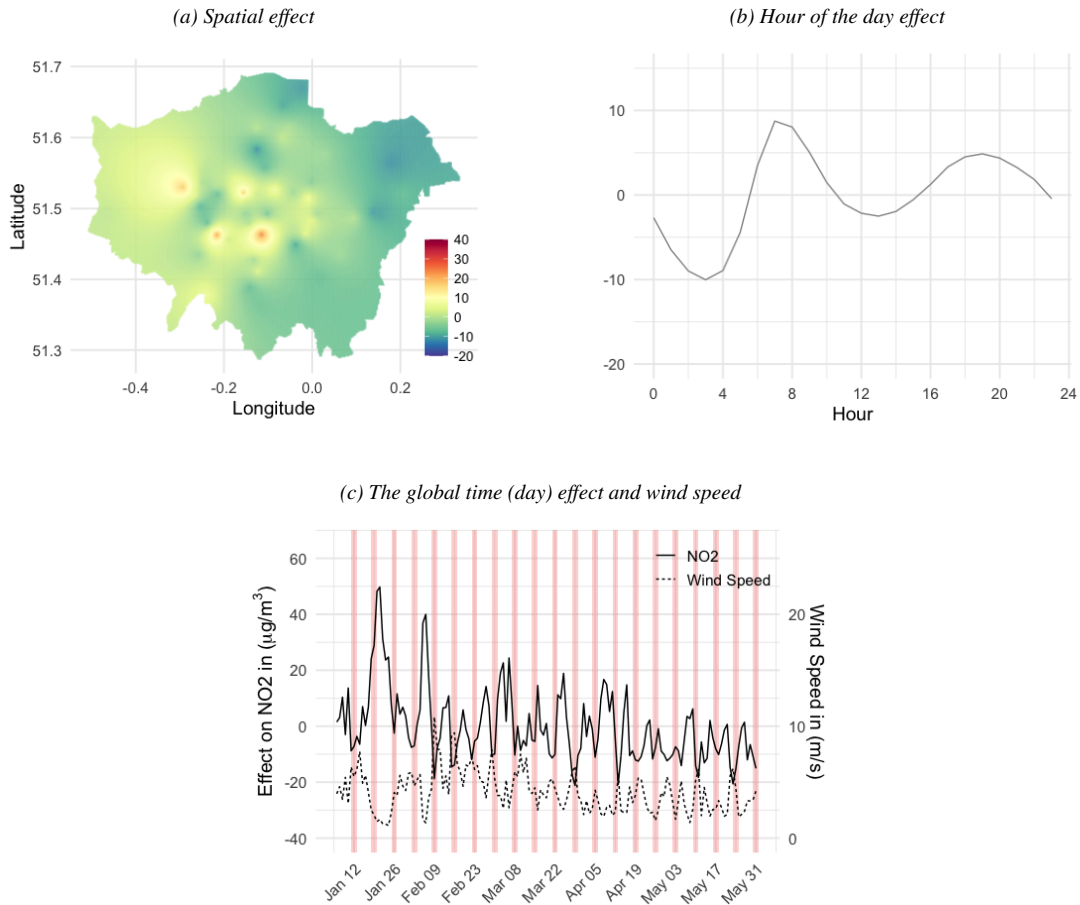


Fig 9: Main effects on NO_2 in $\mu\text{g}/\text{m}^3$. In panel (c), weekends are highlighted. We see low wind speed corresponding to a higher level of pollution.

are many factors to consider in explaining this variation. One possibility is the weekend effect associated with less traffic. Looking at the figure, we see that some troughs in the figure seem to fall into weekend although there are some deviations from this pattern. This may be due to some meteorological factors affecting the concentration level of the pollutant. For example, it is well-known that lower wind speeds are associated with higher concentrations. The two-week period starting on the 12th of January sees one large peak across the sites, which corresponds with the trough in the wind speed. Other weather conditions such as temperature, precipitation or sunlight also affect the levels of NO_2 concentrations in the air. Including meteorological data as covariates can help improve the fit, as well as estimate and visualise the time trend after removing the effect of the weather conditions. If the weekly pattern is still apparent, we can introduce another level in the data structure, i.e., a four-dimensional grid structure, and gain further computational efficiency. The hour of the day effect shown in 9b is averaged over monitoring stations and calendar date. It shows two clear peaks in the morning and in the evening with the former is bigger in magnitude.

As two-way interaction effects between x_3 and both x_1 and x_2 are present, the hour of the day effect changes over location and time. To see this we can plot $\bar{m}_3(x_3) + \bar{m}_{13}(\mathbf{x}_1, x_3)$ and $\bar{m}_3(x_3) + \bar{m}_{23}(x_2, x_3)$ as a function of x_3 for different \mathbf{x}_1 and x_2 . Figure 10 shows

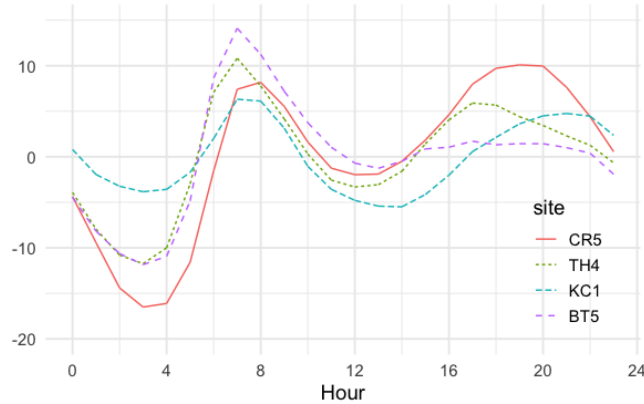


Fig 10: Hour of the day effect on NO_2 in $\mu\text{g}/\text{m}^3$ by site

the estimated daily cycle at selected sites. It is noticeable that Station CR5 and Station TH4 which are located in kerbside and roadside respectively, have two peaks corresponding to rush hours. While the latter (TH4) shows a similar pattern to that of the main effect, the former is distinctively different with a larger peak in the evening. The station in the background, KC1, also shows two peaks but with much smaller magnitude of the effect. Station BT5 is close to an industrial site and with only one peak in the morning. Figure 11 shows the interaction effect between the global time and the hour of the day for selected weeks. During the week commencing on the 27th of January (week 5 of 2020), there are two clear peaks in the beginning of the week, but this pattern becomes less clear over the course of the week. During the weekend, the magnitude of the effect becomes smaller. The week starting on the 23rd of March (week 14 of 2020), where the first COVID-19 lockdown in the UK took place, shows more irregular patterns. The Monday of this week is the day that the British Prime Minister announced the plan to introduce the measure which legally came into force 3 days later. The first national lockdown lasted the next few months with parts of the restriction being lifted from mid-May. The last two plots show the effect in the week starting on the 20-th of April (week 17 of 2020, week 4 of lockdown) and on the 25-th of May (week 22 of 2020, week 11 of lockdown). There is a distinct peak in the morning for many of the days, but the evening peak is much less apparent compared with week 5. Appendix B.4 includes a few more examples of how to visualise and interpret two-way interaction effects.

The chosen model indicates that the change of the cyclical effect over time is different for different location. This can be visualised by plotting $\bar{m}_3(x_3) + \bar{m}_{23}(x_2, x_3) + \bar{m}_{123}(\mathbf{x}_1, x_2, x_3)$ as a function of x_3 (shown in Figure 12). In week 5 of 2020, the pattern in Station CR5 and KC1 are similar especially in the beginning of the week. On the eleventh week into the lockdown, the pattern for Station KC1 is similar to the last panel in Figure 11, while this is not the case for Station CR5, where two daily peaks are still observed.

5. Discussion. This paper proposed a class of Additive GP models using saturated and hierarchical ANOVA decomposition kernels. This is a natural way of constructing additive models that allow for modelling main effects and interaction effects without increasing the number of model parameters. As a class of additive models, the proposed models have good interpretability. This is enhanced by centring kernels, which gives meaningful interpretation on all main and interaction terms included in the model. Furthermore, we showed that with kernels being centred, the popular Kronecker product approach can be extended to handle various structures of interaction effect models. This allows for the analysis of large-scale multidimensional grid data without being constrained to the saturated model.

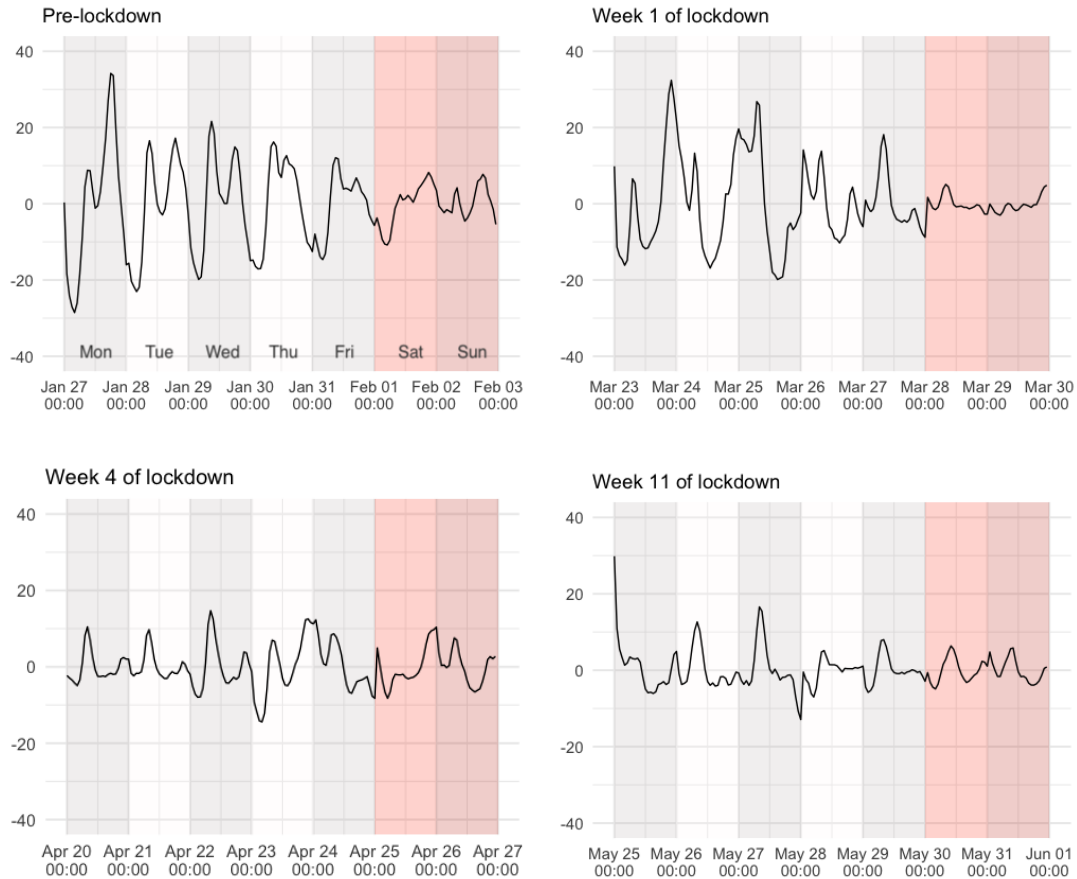


Fig 11: Change in hour of the day effect (in $\mu\text{g}/\text{m}^2$) over time averaged over different monitoring stations.

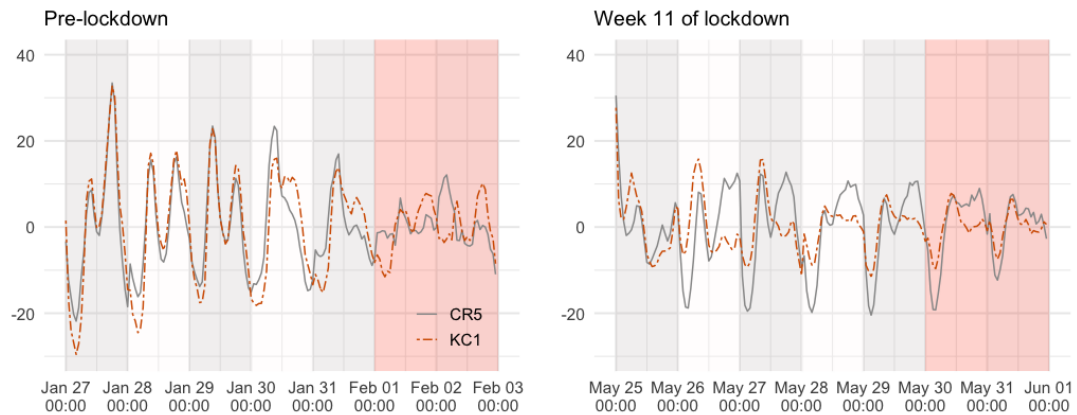


Fig 12: Change in hour of the day effect (in $\mu\text{g}/\text{m}^2$) over time at two different monitoring stations, CR5 and KC1

The proposed method is applied to efficiently analyse hourly-recorded ambient NO₂ concentrations in London for the period covering both before and after the COVID-19 lockdown measure was introduced. We treated the data as three-dimensional grid data, with the location of the monitoring stations, day, and hour of the day as three predictors. The effect of three variables can be seen as the spatial effect, global time effect and daily cyclical effect

respectively. We considered five regression models, including the main effect model, two kinds of two-way (hierarchical) interaction models, the three-way (hierarchical) interaction model, and the three-way interaction only model. We compared the models in terms of the marginal likelihood and found that the three-way interaction model is the best fit for the data, suggesting that the global time trend and the daily cycle are different for different locations, with the latter changing over time. How daily cycles changes over the course of the period differs across various monitoring stations. The proposed Kronecker approach enabled efficient implementation of all models considered. This allowed us to compare different models and confirm the presence of interaction terms. It is also important to note that the success of our approach does not reduce the significance of other scalable approaches to GP regression that can be used for more general data structures such as a subset of data, Nyström approximation, inducing points methods, sparse variational methods, or vice versa. In fact, the Kronecker approach, including our proposal, can be combined with such methods, which can then facilitate the analysis of even larger datasets.

We would like to point out that, while it is not considered in our data analysis, the inclusion of other covariates such as information related to monitoring stations, or meteorological variables is possible under the proposed model. If the covariates are level specific, e.g. types of the monitoring stations (roadside, background etc.) at the top level, or daylight time in London at the middle level, we can simply add the centred covariance function for each covariate to the kernel given at each level, which in this example, are the kernels for location and day, respectively. However, many meteorological variables are observed at a cross-level. For example, we may want to use hourly-recorded wind speed or precipitation at different locations. If the effect of these meteorological variables is assumed linear (including polynomial), we can incorporate them into a model while still avoiding cubic time complexity, by combining the idea of modelling explicit basis functions (Rasmussen and Williams, 2006, Chapter 2.7) with our Kronecker approach. Using such information in the model is especially important if prediction is the main interest. In this case, we should consider additional model assessment criteria to marginal likelihood that is more targeted at predictive accuracy, such as mean squared error or log loss for test data.

Another worthwhile aspect to investigate is the challenge of handling missing values. In this paper, we assume a complete grid structure, i.e., no missing values. This may not always be a reasonable assumption for real-world applications. For example, in air quality monitoring, there may be some periods where the data is not available due to malfunctioning of monitoring devices. Repeated measurements in social, psychological, or medical science commonly suffer from dropout. In this paper, we excluded some monitoring sites that have many missing records and imputed the rest of the missing values by a simple procedure. If the proportion of missing values in the data is large, more sophisticated approaches should be considered to avoid potential bias. Gilboa, Saatçi and Cunningham (2013); Wilson et al. (2014) proposed an approximation to the likelihood in the presence of missing values in multidimensional grid structure data. Our future work will focus on this issue. In particular, the proposed method can be incorporated into an algorithm that sequentially imputes missing values and estimates model parameters.

APPENDIX A: METHODOLOGY

A.1. Posterior in GPR. Let us consider the regression model considered in Section 2.4, i.e., we have

$$\mathbf{y} = (y_1, \dots, y_n)^\top \sim \text{MVN}_n(\mathbf{0}, \mathbf{K} + \sigma^2 \mathbf{I}).$$

Let us assume that we have $\mathbf{x}_j^* \in \mathcal{X}$ for $j = 1, \dots, m$. This set of \mathbf{x}_j^* can include \mathbf{x}_i in a sample (training set). We denote $\mathbf{f}^* = (f(\mathbf{x}_1^*), \dots, f(\mathbf{x}_m^*))$. From our prior we know

$$\mathbf{f}^* \sim \text{MVN}_m(\mathbf{0}, \mathbf{K}_{**}) \quad (\text{A.1})$$

where $\mathbf{K}_{**} = \{k_{i,j}^{**}\}_{m \times m}$ and $k_{i,j}^{**} = k(\mathbf{x}_i^*, \mathbf{x}_j^*)$. Hence we have

$$\begin{bmatrix} \mathbf{y} \\ \mathbf{f}^* \end{bmatrix} \sim \text{MVN}_{n+m} \left(\begin{bmatrix} \mathbf{0} \\ \mathbf{0} \end{bmatrix}, \begin{bmatrix} \mathbf{K} + \sigma^2 \mathbf{I} & \mathbf{K}_* \\ \mathbf{K}_*^\top & \mathbf{K}_{**} \end{bmatrix} \right)$$

where $\mathbf{K}_* = \{k_{*i,j}\}_{n \times m}$ and $k_{*i,j} = k(\mathbf{x}_i, \mathbf{x}_j^*)$. By conditional distribution of multivariate normal distribution,

$$\mathbf{f}^* | \mathbf{X}, \mathbf{X}^*, \mathbf{y} \sim \text{MVN}_m(\boldsymbol{\mu}^*, \mathbf{V}^*)$$

where

$$\begin{aligned} \boldsymbol{\mu}^* &= \mathbf{K}^{*\top} (\mathbf{K} + \sigma^2 \mathbf{I})^{-1} \mathbf{y} \\ \mathbf{V}^* &= \mathbf{K}_{**} - \mathbf{K}^{*\top} (\mathbf{K} + \sigma^2 \mathbf{I})^{-1} \mathbf{K}_* \end{aligned}$$

It is easy to see that we have $\boldsymbol{\mu}^* = (\bar{m}(\mathbf{x}_1^*), \dots, \bar{m}(\mathbf{x}_m^*))$ and $\mathbf{V}^* = \{v_{i,j}^*\}_{m \times m}$ with $v_{i,j}^* = \bar{k}(\mathbf{x}_i^*, \mathbf{x}_j^*)$ where $\bar{m} : \mathcal{X} \rightarrow \mathbb{R}$ and $\bar{k} : \mathcal{X} \times \mathcal{X} \rightarrow \mathbb{R}$ are given by

$$\begin{aligned} \bar{m}(\mathbf{x}) &= \mathbf{k}(\mathbf{x})^\top (\mathbf{K} + \sigma^2 \mathbf{I})^{-1} \mathbf{y}, & \mathbf{x} \in \mathcal{X} \\ \bar{k}(\mathbf{x}, \mathbf{x}') &= k(\mathbf{x}, \mathbf{x}') - \mathbf{k}(\mathbf{x})^\top (\mathbf{K} + \sigma^2 \mathbf{I})^{-1} \mathbf{k}(\mathbf{x}'), & \mathbf{x}, \mathbf{x}' \in \mathcal{X}. \end{aligned}$$

By Kolmogorov extension theorem and Definition 2, this implies that the posterior is the Gaussian process $\text{GP}(\bar{m}, \bar{k})$.

A.2. Centring of kernels and interpretation. Consider a regression model for a real-valued response y and two predictors $\mathbf{x}_1 \in \mathcal{X}_1$ and $\mathbf{x}_2 \in \mathcal{X}_2$ as specified by (2.1) and (2.3). Repeating the latter, the regression function is

$$f(\mathbf{x}_{1i}, \mathbf{x}_{2i}) = a + f_1(\mathbf{x}_{1i}) + f_2(\mathbf{x}_{2i}) + f_{12}(\mathbf{x}_{1i}, \mathbf{x}_{2i})$$

for $i = 1, \dots, n$. The prior over the regression function f is additive GP with saturated ANOVA decomposition kernel (2.7),

$$k((\mathbf{x}_1, \mathbf{x}_2), (\mathbf{x}'_1, \mathbf{x}'_2)) = 1 + k_1(\mathbf{x}_1, \mathbf{x}'_1) + k_2(\mathbf{x}_2, \mathbf{x}'_2) + k_1(\mathbf{x}_1, \mathbf{x}'_1)k_2(\mathbf{x}_2, \mathbf{x}'_2),$$

where we assume that each base kernel k_l for $l = 1, 2$ is empirically centred and $\alpha_0 = 1$ for simplicity. We write the Gram matrix $\mathbf{K} = \mathbf{1}_n \mathbf{1}_n^\top + \mathbf{K}_1 + \mathbf{K}_2 + \mathbf{K}_1 \circ \mathbf{K}_2$. Due to centring, we have $\mathbf{K}_1 \mathbf{1}_n = \mathbf{K}_2 \mathbf{1}_n = \mathbf{0}$. Using (2.17), the posterior mean function is sum of $\bar{m}_a = \mathbf{1}_n^\top \mathbf{w}$ which corresponds with the constant term, and

$$\begin{aligned} \bar{m}_1(\mathbf{x}_1) &= \mathbf{k}_1(\mathbf{x}_1)^\top \mathbf{w} & \mathbf{x}_1 \in \mathcal{X}_1 \\ \bar{m}_2(\mathbf{x}_2) &= \mathbf{k}_2(\mathbf{x}_2)^\top \mathbf{w} & \mathbf{x}_2 \in \mathcal{X}_2 \\ \bar{m}_{12}(\mathbf{x}_1, \mathbf{x}_2) &= (\mathbf{k}_1(\mathbf{x}_1) \circ \mathbf{k}_2(\mathbf{x}_2))^\top \mathbf{w} & \mathbf{x}_1 \in \mathcal{X}_1, \mathbf{x}_2 \in \mathcal{X}_2 \end{aligned}$$

where $\mathbf{w} = (\mathbf{K} + \sigma^2 \mathbf{I})^{-1} \mathbf{y}$ and $\mathbf{k}_l(\mathbf{x}_l) = (k_l(\mathbf{x}_l, \mathbf{x}_1), \dots, k_l(\mathbf{x}_l, \mathbf{x}_n))^\top$ for $l = 1, 2$. Each \bar{m}_j corresponds with the term f_j for $j \in \{1, 2, 12\}$.

A.2.1. Properties of posterior mean functions. Centring kernels implies that each of the posterior mean functions for main terms sums to zero over each input, i.e., $\sum_{i=1}^n \bar{m}_1(\mathbf{x}_{1i}) = \sum_{i=1}^n \bar{m}_2(\mathbf{x}_{2i}) = 0$. We can see this by

$$\sum_{i=1}^n \bar{m}_l(\mathbf{x}_{li}) = \underbrace{\mathbf{1}_n^\top \mathbf{K}_l}_{=\mathbf{0}^\top} \mathbf{w} = 0$$

for $l = 1, 2$. For interaction terms, we have a similar property, but the summation is over one input, e.g., $\sum_{i=1}^n \bar{m}_{12}(\mathbf{x}_{1i}, \mathbf{x}_2) = 0$. We show this by

$$\begin{aligned} \sum_{i=1}^n \bar{m}_{12}(\mathbf{x}_{1i}, \mathbf{x}_2) &= \mathbf{1}_n^\top (\mathbf{K}_1 \bullet \mathbf{k}_2(\mathbf{x}_2))^\top \mathbf{w} = \mathbf{1}_n^\top (\mathbf{k}_2(\mathbf{x}_2) \bullet \mathbf{K}_1)^\top \mathbf{w} \\ &= \mathbf{1}_n^\top (\mathbf{D}_{k_2} \mathbf{K}_1)^\top \mathbf{w} = \underbrace{\mathbf{1}_n^\top \mathbf{K}_1}_{=\mathbf{0}^\top} \mathbf{D}_{k_2} \mathbf{w} = 0 \end{aligned}$$

where \bullet is row-wise Kronecker product (see Section 3.3 of the Supplementary Material (Ishida and Bergsma, 2023)) and $\mathbf{D}_{k_2} = \text{diag}(\mathbf{k}_2(\mathbf{x}_2))$. We can show $\sum_{i=1}^n \bar{m}_{12}(\mathbf{x}_1, \mathbf{x}_{2i}) = 0$ in a similar manner. Interestingly, the summation over both inputs does not equal 0 in general i.e., $\sum_{i=1}^n \bar{m}_{12}(\mathbf{x}_{1i}, \mathbf{x}_{2i}) \neq 0$. The exception is when we have multi-dimensional grid data, as introduced in Section 3. Then we have $\sum_{i=1}^{n_1} \sum_{j=1}^{n_2} \bar{m}_{12}(\mathbf{x}_{1i}, \mathbf{x}_{2j}) = 0$ where \bar{m}_{12} now corresponds with the last term in (3.3).

A.2.2. Interpretation. These properties of posterior mean functions allow for meaningful interpretation of each main and interaction term. To see this, we start by interaction term. We can understand how the effect of \mathbf{x}_1 changes depending on the level of \mathbf{x}_2 by plotting

$$g(\mathbf{x}_1 | \mathbf{x}_2) := \bar{m}_1(\mathbf{x}_1) + \bar{m}_{12}(\mathbf{x}_1, \mathbf{x}_2) \quad (\text{A.2})$$

as a function of \mathbf{x}_1 for a fixed value of $\mathbf{x}_2 \in \mathcal{X}_2$. Let us now evaluate this function at each observed value $\mathbf{x}_{2,i}$ for $i = 1, \dots, n$, and take the average. We have that

$$\frac{1}{n} \sum_{i=1}^n g(\mathbf{x}_1 | \mathbf{x}_{2i}) = \bar{m}_1(\mathbf{x}_1) + \underbrace{\frac{1}{n} \sum_{i=1}^n \bar{m}_{12}(\mathbf{x}_1, \mathbf{x}_{2i})}_{=0} = \bar{m}_1(\mathbf{x}_1).$$

This allows for interpreting the main effect term $\bar{m}_1(\mathbf{x}_1)$ in the interaction model as the effect of \mathbf{x}_1 averaged over each input of \mathbf{x}_2 . We can generalise this to a higher order interaction case. For example, if we have the third predictor $\mathbf{x}_3 \in \mathcal{X}_3$, and include the three-way interaction term in the regression model, we can show that $\sum_{i=1}^n \bar{m}_{123}(\mathbf{x}_1, \mathbf{x}_2, \mathbf{x}_{3i}) = 0$, for $\mathbf{x}_1 \in \mathcal{X}_1$, $\mathbf{x}_2 \in \mathcal{X}_2$. Then the interpretation of the two-way interaction effect $\bar{m}_{12}(\mathbf{x}_1, \mathbf{x}_2)$ stays the same as the example above (A.2), but now averaged over each input of \mathbf{x}_3 . The posterior mean of the constant term, \bar{m}_a , has an interpretation as the average of the posterior mean of the response \mathbf{y} after averaging over all (main and interaction) effects, under two circumstances: 1) when we have multi-dimensional grid data, or 2) when we have main effects only model with non-structured data.

A.3. eigendecomposition of a centred Gram matrix. Consider a $n \times n$ Gram \mathbf{K}^c matrix given by a centred kernel function (2.10). In what follows we show that a centred Gram matrix has an eigendecomposition of a special form. We write an eigendecomposition of a matrix \mathbf{M} by $\mathbf{M} = \mathbf{Q}\mathbf{\Lambda}\mathbf{Q}^\top$ where $\mathbf{\Lambda}$ is a diagonal matrix of which diagonal elements are eigenvalues of \mathbf{M} in non-decreasing order and \mathbf{Q} is an orthonormal matrix with its i -th column \mathbf{q}_i being the eigenvector which corresponds to i -th eigenvalue. For a centred Gram matrix, we have the following.

LEMMA 2. Any eigenvector \mathbf{q}_i of a $n \times n$ centred Gram matrix $\mathbf{K}^{(c)}$ associated with non-zero eigenvalue λ_i is orthogonal to $\mathbf{1}_n$.

PROOF. Using $\mathbf{K}^{(c)}\mathbf{q}_i = \lambda_i\mathbf{q}_i$, we have

$$\mathbf{q}_i^\top \mathbf{1}_n = \frac{1}{\lambda_i} \mathbf{q}_i^\top \mathbf{K}^{(c)} \mathbf{1}_n = \mathbf{0}.$$

The last equality is due to the fact that all rows and columns of a centred matrix sum to 0. \square

LEMMA 3. Any $n \times n$ centred Gram matrix $\mathbf{K}^{(c)}$ has the following eigendecomposition:

$$\mathbf{K}^{(c)} = \mathbf{Q}^{(c)} \mathbf{\Lambda}^{(c)} \mathbf{Q}^{(c)\top} \quad (\text{A.3})$$

where

$$\mathbf{\Lambda}^{(c)} = \text{diag} \left((0, \lambda_2, \dots, \lambda_n)^\top \right), \lambda_j \geq 0 \forall j \in \{2, \dots, n\} \quad (\text{A.4})$$

and

$$\mathbf{Q}^{(c)} = \begin{bmatrix} \frac{1}{\sqrt{n}} & & & \\ \vdots & \mathbf{q}_2 & \cdots & \mathbf{q}_n \\ \frac{1}{\sqrt{n}} & & & \end{bmatrix}. \quad (\text{A.5})$$

PROOF. Let k denote the number of zero eigenvalues of $\mathbf{K}^{(c)}$. Due to the centring, $\text{rank}(\mathbf{K}^{(c)}) \leq n - 1$, i.e., we have $k \geq 1$.

For $k = 1$, we have $\lambda_j > 0, \forall j \in \{2, \dots, n\}$ and the eigenvectors $\mathbf{q}_2, \dots, \mathbf{q}_n$ are orthogonal to $\mathbf{1}_n$ from Lemma 2. Normalising the vector $\mathbf{1}_n$ completes an orthonormal basis, hence the first column of $\mathbf{Q}^{(c)}$ is given by $\frac{1}{\sqrt{n}}\mathbf{1}$.

For $k \geq 2$, the first k columns of $\mathbf{Q}^{(c)}$, $(\mathbf{q}_1, \dots, \mathbf{q}_k)$, are not uniquely determined. Using $\mathbf{q}_j^\top (\frac{1}{\sqrt{n}}\mathbf{1}_n) = \frac{1}{\sqrt{n}}\mathbf{q}_j^\top \mathbf{1}_n = \mathbf{0}$ for $j = k + 1, \dots, n$, we set $\mathbf{q}_1 = \frac{1}{\sqrt{n}}\mathbf{1}_n$ and find $(\mathbf{q}_2, \dots, \mathbf{q}_k)$ to complete an orthonormal system. \square

In practice, we may use a computer program to obtain a initial set of normalised eigenvectors denoted by $\mathbf{v}_1, \dots, \mathbf{v}_n$. For $k \geq 2$, $\mathbf{v}_1, \dots, \mathbf{v}_k$ may not contain a vector $\frac{1}{\sqrt{n}}\mathbf{1}_n$ but $\text{span}(\mathbf{v}_1, \dots, \mathbf{v}_k)$ contains $\mathbf{1}_n$. To have orthonormal bases $\mathbf{q}_1, \dots, \mathbf{q}_n$ specified above, we take $\mathbf{q}_1 = \frac{1}{\sqrt{n}}\mathbf{1}_n$ and $\mathbf{q}_j = \mathbf{v}_j$ for $j = k + 1, \dots, n$. The rest of the vectors $\mathbf{q}_2, \dots, \mathbf{q}_k$ can be computed using for example Gram–Schmidt process.

REMARK 1. The $n \times n$ matrix $\mathbf{1}_n \mathbf{1}_n^\top$ has the following decomposition:

$$\mathbf{1}_n \mathbf{1}_n^\top = \mathbf{Q}^{(c)} \mathbf{A}_n \mathbf{Q}^{(c)\top} \quad (\text{A.6})$$

where $\mathbf{Q}^{(c)}$ is given by (A.5) and \mathbf{A}_n is a $n \times n$ matrix with i, i -th element n and 0 everywhere else, i.e.,

$$\mathbf{A}_n = \begin{bmatrix} n & 0 & \cdots & 0 \\ 0 & 0 & \cdots & 0 \\ \vdots & \vdots & \ddots & \vdots \\ 0 & 0 & \cdots & 0 \end{bmatrix}. \quad (\text{A.7})$$

APPENDIX B: DATA ANALYSIS

B.1. Data manipulation.

TABLE 2
Adjustment from GMT to BST

Original time in GMT	Original y	Time in BST	Adjusted time	y after adjustment
\vdots	\vdots	\vdots	\vdots	\vdots
2020-03-29 0:00AM	y_{t-1}	-	2020-03-29 0:00AM	y_{t-1}
2020-03-29 1:00AM	y_t	2020-03-29 2:00AM	2020-03-29 1:00AM	$(y_{t-1} + y_t)/2$
2020-03-29 2:00AM	y_{t+1}	2020-03-29 3:00AM	2020-03-29 2:00AM	y_t
2020-03-29 3:00AM	y_{t+1}	2020-03-29 3:00AM	2020-03-29 3:00AM	y_{t+1}
\vdots	\vdots	\vdots	\vdots	\vdots

Missing value imputation. In the dataset used in this paper, we had 1,290 missing value out of 208,152. For each missing value at a measurement site, we created a small subset of the data consisting of the observations collected from the same site from 24 hours before to 24 hours after the missing values is observed. A simple one dimensional Gaussian process regression with squared and centred standard ($\gamma = \frac{1}{2}$) Brownian Motion kernel is then fitted. We replace the missing value with the posterior predictive mean given by (2.15).

Adjustment of Summer time. The study period, which spans from the 6th of January 2020 to the 31st of May, 2020, includes the clock change to British Summer Time (BST), started on 1:00 AM on March 29. The timestamp in the original data are all in Greenwich Mean Time (GMT). We converted the timestamp to match BST from 1:00 AM (in GMT) forward. This resulted in one hour gap without any record at 1:00 AM of the adjusted timestamp. We filled the gap with a mean of the record before and after. The procedure is summarised in Table 2.

B.2. Gram matrix for each models. Let \mathbf{K}_l denote the Gram matrix that corresponds with the kernel k_l in Section 4.2, i.e., $\mathbf{K}_l = \{k_{i,j}^{(l)}\}_{1 \leq i,j \leq n_l}$. The Gram matrices for the models under consideration in Section 4.2 are listed as follows.

- Model 1: main effect

$$\mathbf{K}_{m1} = \bigotimes_{l=1}^3 \mathbf{1}_{n_l} \mathbf{1}_{n_l}^\top + \mathbf{K}_1 \otimes \mathbf{1}_{n_2} \mathbf{1}_{n_2}^\top \otimes \mathbf{1}_{n_3} \mathbf{1}_{n_3}^\top + \mathbf{1}_{n_1} \mathbf{1}_{n_1}^\top \otimes \mathbf{K}_2 \otimes \mathbf{1}_{n_3} \mathbf{1}_{n_3}^\top + \mathbf{1}_{n_1} \mathbf{1}_{n_1}^\top \otimes \mathbf{1}_{n_2} \mathbf{1}_{n_2}^\top \otimes \mathbf{K}_3$$

- Model 2: space-time interactions

$$\mathbf{K}_{m2} = \mathbf{K}_{m1} + \mathbf{K}_1 \otimes \mathbf{K}_2 \otimes \mathbf{1}_{n_3} \mathbf{1}_{n_3}^\top + \mathbf{K}_1 \otimes \mathbf{1}_{n_2} \mathbf{1}_{n_2}^\top \otimes \mathbf{K}_3$$

- Model 3: all two-way interactions

$$\mathbf{K}_{m3} = \mathbf{K}_{m2} + \mathbf{1}_{n_1} \mathbf{1}_{n_1}^\top \otimes \mathbf{K}_2 \otimes \mathbf{K}_3$$

- Model 4: saturated

$$\mathbf{K}_{m4} = \mathbf{K}_{m3} + \mathbf{K}_1 \otimes \mathbf{K}_2 \otimes \mathbf{K}_3 = \bigotimes_{l=1}^3 \left(\mathbf{1}_{n_l} \mathbf{1}_{n_l}^\top + \mathbf{K}_l \right)$$

- Model 5: three-way interaction only

$$\mathbf{K}_{m5} = \mathbf{K}_1 \otimes \mathbf{K}_2 \otimes \mathbf{K}_3$$

TABLE 3

The parameter estimates obtained by maximising the log-marginal likelihood using L-BFGS algorithm provided in Stan. The time taken (in seconds) until convergence is also provided.

Model	α_0	α_1	α_2	α_3	σ	Time(s)
1: main	6.863	5.024	2.197	0.319	14.850	3.41
2: spatio-temporal interaction	14.401	1.284	0.672	0.235	12.537	4.07
3: all two-way interaction	10.633	1.865	1.320	0.306	8.367s	4.23
4: saturated	52.024	0.482	0.942	0.0512	6.508	3.41
5: three-way interaction only	-	0.000790	-	-	36.429	1.36

B.3. Hyper-parameter estimation by Naive Bayes. In addition to obtaining samples from the posterior of the hyper-parameters, we also estimated the hyper-parameters by finding the maximiser of the log marginal likelihood (2.19). We used optimisation algorithm provided by Stan which can be run with the same code used for MCMC sampling. The convergence was achieved within a few seconds for all models. The values obtained (Table 3) are close to those of the MCMC sample mean.

B.4. Visualisation of interaction effects. The selected model implies that the effect of x_2 (the global time effect) takes on different forms for different values of \mathbf{x}_1 (location). This is shown in Figure 13, which plot $\bar{m}_2(x_2) + \bar{m}_{12}(\mathbf{x}_1, x_2)$ as a function x_2 given a set of coordinates \mathbf{x}_1 at selected stations. Figure 14 shows how the spatial effect changes over the course of a day. These are the plots of $\bar{m}_1(\mathbf{x}_1) + \bar{m}_{13}(\mathbf{x}_1, x_3)$ as a function of \mathbf{x}_1 evaluated at different hours of the day.

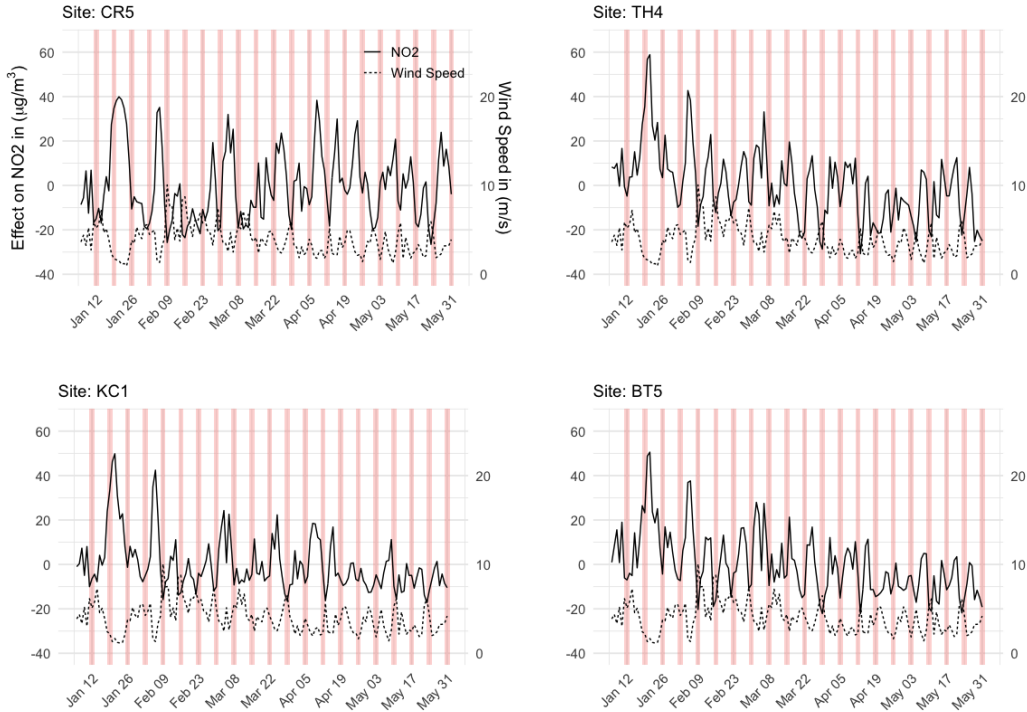


Fig 13: The global time (day) effect and wind speed by site with weekends highlighted. The effect is averaged over hour of the day.

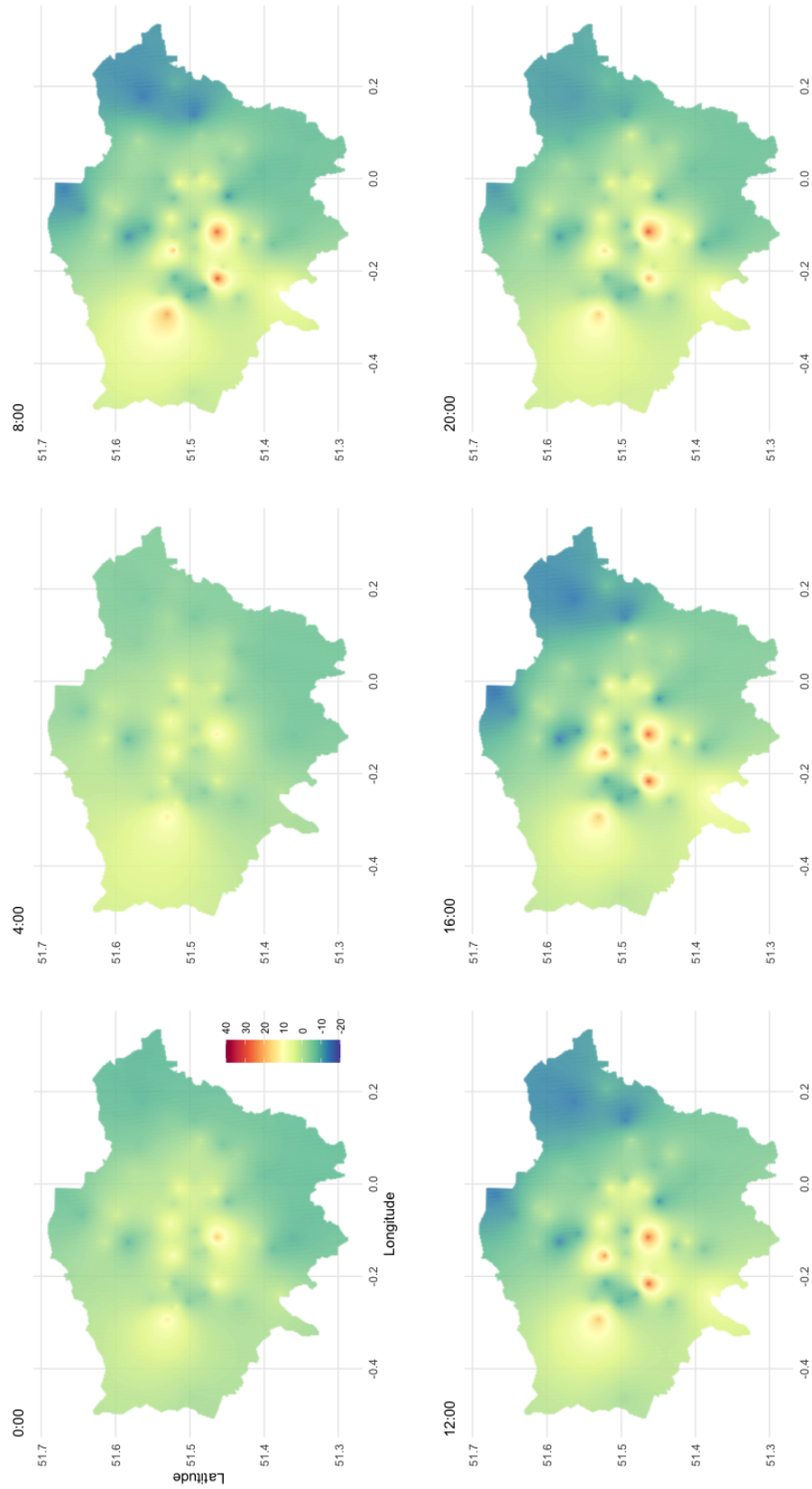


Fig 14: The spatial effect over London at different hours of the day averaged over different calendar dates. The effect is measured in $\mu\text{g}/\text{m}^3$.

SUPPLEMENTARY MATERIAL

Data and code for data analysis

The zip folder contains NO₂ concentration data used in this paper and code (Stan files and an R file) implementing the proposed methodology for the dataset.

Supplement to "Efficient and Interpretable Additive Gaussian Process Regression and Application to Analysis of Hourly-recorded NO₂ Concentrations in London"

Additional information on different kernels, and the concept of kernel centring as well as properties of Kronecker product is included in the pdf file.

REFERENCES

- ADLER, R. J. (1981). *The geometry of random fields*. John Wiley & Sons.
- BERGSMA, W. (2020). Regression with I-priors. *Econometrics and Statistics* **14** 89–111.
- BERGSMA, W. and JAMIL, H. (2023). Additive interaction modelling using I-priors. *arXiv preprint arXiv:2007.15766*.
- CAMELETTI, M. (2020). The effect of corona virus lockdown on air pollution: Evidence from the city of Brescia in Lombardia region (Italy). *Atmospheric Environment* **239** 117794.
- COOPER, M. J., MARTIN, R. V., HAMMER, M. S., LEVELT, P. F., VEEFKIND, P., LAMSAL, L. N., KROTKOV, N. A., BROOK, J. R. and MCLINDEN, C. A. (2022). Global fine-scale changes in ambient NO₂ during COVID-19 lockdowns. *Nature* **601** 380–387.
- DATTA, A., BANERJEE, S., FINLEY, A. O., HAMM, N. A. and SCHAAP, M. (2016). Nonseparable dynamic nearest neighbor Gaussian process models for large spatio-temporal data with an application to particulate matter analysis. *The annals of applied statistics* **10** 1286.
- DIGGLE, P. J., MORAGA, P., ROWLINGSON, B. and TAYLOR, B. M. (2013). Spatial and spatio-temporal log-Gaussian Cox processes: extending the geostatistical paradigm. *Statistical Science* 542–563.
- DURRANDE, N., GINSBOURGER, D., ROUSTANT, O. and CARRARO, L. (2013). ANOVA kernels and RKHS of zero mean functions for model-based sensitivity analysis. *Journal of Multivariate Analysis* **115** 57–67.
- DUTTA, V., KUMAR, S. and DUBEY, D. (2021). Recent advances in satellite mapping of global air quality: evidences during COVID-19 pandemic. *Environmental Sustainability* 1–19.
- DUVENAUD, D., NICKISCH, H. and RASMUSSEN, C. (2011). Additive Gaussian Processes. In *Advances in Neural Information Processing Systems* **24**.
- EMBRECHTS, P. and MAEJIMA, M. (2002). Selfsimilar Processes, Princeton Ser. *Appl. Math., Princeton University Press, Princeton, NJ*.
- FIORAVANTI, G., CAMELETTI, M., MARTINO, S., CATTANI, G. and PISONI, E. (2022). A spatiotemporal analysis of NO₂ concentrations during the Italian 2020 COVID-19 lockdown. *Environmetrics* **33** e2723.
- FLAXMAN, S., WILSON, A., NEILL, D., NICKISCH, H. and SMOLA, A. (2015). Fast Kronecker inference in Gaussian processes with non-Gaussian likelihoods. In *International conference on machine learning* 607–616. PMLR.
- GENTON, M. G. (2001). Classes of kernels for machine learning: a statistics perspective. *Journal of machine learning research* **2** 299–312.
- GILBOA, E., SAATÇI, Y. and CUNNINGHAM, J. P. (2013). Scaling multidimensional inference for structured Gaussian processes. *IEEE transactions on pattern analysis and machine intelligence* **37** 424–436.
- GRANCHAROVA, A., KOČIJAN, J. and JOHANSEN, T. A. (2008). Explicit stochastic predictive control of combustion plants based on Gaussian process models. *Automatica* **44** 1621–1631.
- GROOT, P., PETERS, M., HESKES, T. and KETTER, W. (2014). Fast Laplace approximation for Gaussian processes with a tensor product kernel.
- GU, C. (2002). *Smoothing spline ANOVA models* **297**. Springer.
- HASTIE, T. and TIBSHIRANI, R. (1990). *Generalized additive models*. Wiley Online Library.
- HENSMAN, J., FUSI, N. and LAWRENCE, N. D. (2013). Gaussian processes for big data. In *Uncertainty in Artificial Intelligence* 282. Citeseer.
- HIGHAM, J., RAMÍREZ, C. A., GREEN, M. and MORSE, A. (2021). UK COVID-19 lockdown: 100 days of air pollution reduction? *Air Quality, Atmosphere & Health* **14** 325–332.
- ISHIDA, S. and BERGSMA, W. (2023). Supplement to "Efficient Additive Gaussian Process Regression for Large-scale Data and Application to Analysis of Hourly-recorded NO₂ Concentrations in London".
- JAMIL, H. (2018). Regression modelling using priors depending on Fisher information covariance kernels (I-priors), PhD thesis, London School of Economics and Political Science.

- JAMIL, H. and BERGSMA, W. (2020). Bayesian Variable Selection for Linear Models Using I-Priors. In *Theoretical, Modelling and Numerical Simulations Toward Industry 4.0* 107–132. Springer.
- JEPHCOTE, C., HANSELL, A. L., ADAMS, K. and GULLIVER, J. (2021). Changes in air quality during COVID-19 ‘lockdown’ in the United Kingdom. *Environmental Pollution* **272** 116011.
- KRIGE, D. G. (1951). A statistical approach to some basic mine valuation problems on the Witwatersrand. *Journal of the Chemical, Metallurgical and Mining Society of South Africa* **52** 119–139.
- LEE, D. (2011). A comparison of conditional autoregressive models used in Bayesian disease mapping. *Spatial and spatio-temporal epidemiology* **2** 79–89.
- LEE, J. D., DRYSDALE, W. S., FINCH, D. P., WILDE, S. E. and PALMER, P. I. (2020). UK surface NO₂ levels dropped by 42% during the COVID-19 lockdown: impact on surface O₃. *Atmospheric Chemistry and Physics* **20** 15743–15759.
- LIU, H., YANG, C., HUANG, M., WANG, D. and YOO, C. (2018). Modeling of subway indoor air quality using Gaussian process regression. *Journal of hazardous materials* **359** 266–273.
- LIU, H., ONG, Y.-S., SHEN, X. and CAI, J. (2020). When Gaussian process meets big data: A review of scalable GPs. *IEEE transactions on neural networks and learning systems* **31** 4405–4423.
- MACKAY, D. J. (1995). Probable networks and plausible predictions—a review of practical Bayesian methods for supervised neural networks. *Network: computation in neural systems* **6** 469.
- MATHERON, G. (1963). Principles of Geostatistics. *Economic Geology* **58** 1246–1266.
- MELKUMYAN, A. and RAMOS, F. T. (2009). A sparse covariance function for exact Gaussian process inference in large datasets. In *Twenty-first international joint conference on artificial intelligence*.
- MØLLER, J., SYVERSVEEN, A. R. and WAAGEPETERSEN, R. P. (1998). Log Gaussian Cox processes. *Scandinavian journal of statistics* **25** 451–482.
- MURRAY, I. and GHAHRAMANI, Z. (2005). A note on the evidence and Bayesian Occam’s razor. *Gatsby Computational Neuroscience Unit Tech Report* 1–4.
- PATEL, Z. B., PUROHIT, P., PATEL, H. M., SAHNI, S. and BATRA, N. (2022). Accurate and scalable gaussian processes for fine-grained air quality inference. In *Proceedings of the AAAI Conference on Artificial Intelligence* **36** 12080–12088.
- PETELIN, D., GRANCHAROVA, A. and KOČIJAN, J. (2013). Evolving Gaussian process models for prediction of ozone concentration in the air. *Simulation modelling practice and theory* **33** 68–80.
- PINDER, T., HOLLAWAY, M., NEMETH, C., YOUNG, P. J. and LESLIE, D. (2021). A Probabilistic assessment of the COVID-19 lockdown on air quality in the UK. *arXiv preprint arXiv:2104.10979*.
- PLATE, T. A. (1999). Accuracy versus interpretability in flexible modeling: Implementing a tradeoff using gaussian process models. *Behaviormetrika* **26** 29–50.
- RASMUSSEN, C. E. and WILLIAMS, C. K. (2006). *Gaussian processes for machine learning*. MIT press, Cambridge, Mass.
- SAATÇI, Y. (2012). Scalable inference for structured Gaussian process models, PhD thesis, University of Cambridge.
- SOLBERG, S., WALKER, S.-E., SCHNEIDER, P. and GUERREIRO, C. (2021). Quantifying the impact of the Covid-19 lockdown measures on nitrogen dioxide levels throughout Europe. *Atmosphere* **12** 131.
- STITSON, M., GAMMERMAN, A., VAPNIK, V., VOVK, V., WATKINS, C. and WESTON, J. (1999). Support vector regression with ANOVA decomposition kernels. *Advanced in Kernel methods: Support Vector Learning*.
- TITSIAS, M. (2009). Variational learning of inducing variables in sparse Gaussian processes. In *Artificial intelligence and statistics* 567–574. PMLR.
- WAHBA, G., WANG, Y., GU, C., KLEIN, R. and KLEIN, B. (1995). Smoothing spline ANOVA for exponential families, with application to the Wisconsin Epidemiological Study of Diabetic Retinopathy: the 1994 Neyman Memorial Lecture. *The Annals of Statistics* **23** 1865–1895.
- WILLIAMS, C. and SEEGER, M. (2001). Using the Nyström method to speed up kernel machines. *Advances in neural information processing systems* **13**.
- WILSON, A. and NICKISCH, H. (2015). Kernel interpolation for scalable structured Gaussian processes (KISS-GP). In *International conference on machine learning* 1775–1784. PMLR.
- WILSON, A. G., GILBOA, E., NEHORAI, A. and CUNNINGHAM, J. P. (2014). Fast kernel learning for multidimensional pattern extrapolation. *Advances in neural information processing systems* **27**.

SUPPLEMENT TO "EFFICIENT AND INTERPRETABLE ADDITIVE GAUSSIAN PROCESS REGRESSION AND APPLICATION TO ANALYSIS OF HOURLY-RECORDED NO₂ CONCENTRATIONS IN LONDON"

BY SAHOKO ISHIDA^{1,a} AND WICHER BERGSMA^{1,b}

¹Department of Statistics, London School of Economics and Political Science, ^as.ishida@lse.ac.uk; ^bw.p.bergsma@lse.ac.uk

1. Kernels and Kernel properties.

1.1. Different kernels.

Common kernels. We introduced squared exponential kernel and fractional Brownian Motion kernel in the paper. The examples below are other kernels that are commonly used in the machine learning and spatial statistics literature. Note that all kernels have a scale parameter $\alpha > 0$ and some also share another parameter $\rho > 0$, called length-scale. Let $\mathbf{x}, \mathbf{x}' \in \mathbb{R}^m$ and $t, t' \in \mathbb{R}$ and $c > 0$ be a constant.

1. Matérn class kernel (?, ?):

$$k_{mat}(\mathbf{x}, \mathbf{x}') = \alpha^2 \frac{2^{1-\nu}}{\Gamma(\nu)} \left(\frac{\sqrt{2\nu} \|\mathbf{x} - \mathbf{x}'\|}{\rho} \right)^\nu K_\nu \left(\frac{\sqrt{2\nu} \|\mathbf{x} - \mathbf{x}'\|}{\rho} \right),$$

where K_ν is a modified Bessel function. The parameter $\nu > 0$ determines the roughness of the corresponding process.

2. Periodic kernel:

$$k_{pr}(t, t') = \alpha^2 \exp \left(-\frac{2 \sin^2 \left(\frac{\pi |t-t'|}{p} \right)}{\rho^2} \right),$$

where $p > 0$, period parameter, can be treated as known or unknown. Corresponding GP is a periodic function of period p .

3. Polynomial kernel

$$k_{pol}(\mathbf{x}, \mathbf{x}') = \alpha^2 \left(\mathbf{x}^\top \mathbf{x}' + c \right)^d,$$

where $m \in \mathbb{N}$. With $d = 1$ we have linear kernel.

4. Constant kernel

$$k_{const}(\mathbf{x}, \mathbf{x}') = c \tag{1.1}$$

With Matérn class kernels, the smoothness of the process can be controlled by parameter ν . With $\nu = 1.5$ process is rough (see figure 1) compared with $\nu = 2.5$. It is worth noting that for $\nu \rightarrow \infty$, it equals S.E. kernel. Periodic kernel is useful when handling the continuous-time process that has a regular cycle, e.g. daily, weekly or annually. It can be derived from S.E. kernel; we have $k_{se}(\mathbf{u}, \mathbf{u}') = k_{pr}(t, t')$ where $\mathbf{u} = \left(\sin\left(\frac{p}{2\pi}t\right), \cos\left(\frac{p}{2\pi}t\right) \right)^\top$. In fact any kernel k can be made periodic with this formulation. The constant kernel is usually used in combination with other kernels.

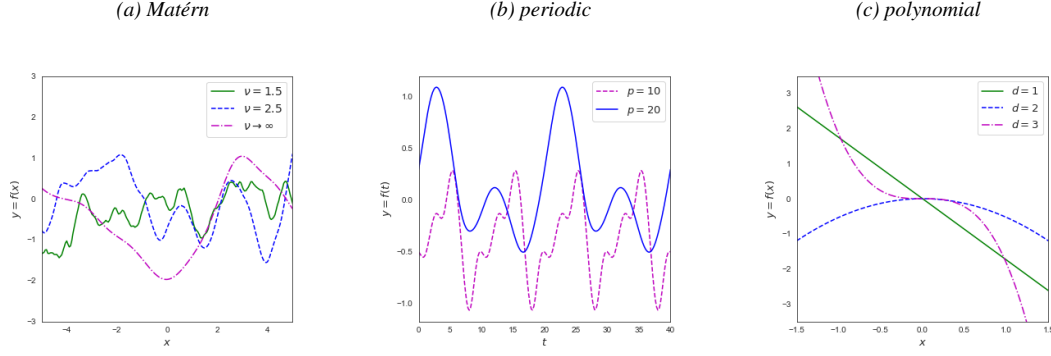


Fig 1: Sample paths from zero mean Gaussian process with different kernels. For all panels, the scale parameter α is set to be 1, and the length-scale parameter $\rho = 1$ for (a) and (b). For polynomial kernel, $c = 0$. For the additional parameters see the legend of each panel.

Stationary and non-stationary kernel. SE kernel, Matérn kernel, and periodic kernel constructed from SE kernel are in the class of stationary kernel, more specifically isotropic kernel. A stationary kernel is a function of a lag vector $\tau = \mathbf{x} - \mathbf{x}'$ of two inputs. When the value of the function depends only on the norm of the two inputs $r = \|\tau\|$, the kernel is said to be isotropic and the corresponding process is invariant under shift in time or space. While the assumption of isotropy or stationarity gives a nice interpretation of correlation structure, we need a class of non-stationary kernels in the case where this assumption does not hold. A few simple examples of non-stationary kernels include linear kernel and polynomial kernel. Using these kernels in Gaussian process regression corresponds with Bayesian linear or polynomial regression. Another useful non-stationary kernel is the fractional Brownian Motion kernel and kernels that are constructed from this kernel, such as its centred version.

1.2. Kernel sums and products. Given valid kernels k_1 and k_2 on \mathcal{X} , a function $k : \mathcal{X} \times \mathcal{X} \rightarrow \mathbb{R}$ constructed as their sum or product

$$k(\mathbf{x}, \mathbf{x}') = k_1(\mathbf{x}, \mathbf{x}') + k_2(\mathbf{x}, \mathbf{x}')$$

$$k(\mathbf{x}, \mathbf{x}') = k_1(\mathbf{x}, \mathbf{x}')k_2(\mathbf{x}, \mathbf{x}')$$

constitutes a positive definite kernel. The kernel k_1 or k_2 can be a (positive) constant kernel (1.1). Hence, adding a positive constant or multiplying by a positive constant gives a positive definite kernel. It is also important to note that it is not necessary that k_1 and k_2 are defined on the same set. For example, given $k_1 : \mathcal{X}_1 \times \mathcal{X}_1 \rightarrow \mathbb{R}$ and $k_2 : \mathcal{X}_2 \times \mathcal{X}_2 \rightarrow \mathbb{R}$, then $k : \mathcal{X} \times \mathcal{X} \rightarrow \mathbb{R}$ where $\mathcal{X} = \mathcal{X}_1 \times \mathcal{X}_2$ given by

$$k((\mathbf{x}_1, \mathbf{x}_2), (\mathbf{x}'_1, \mathbf{x}'_2)) = 1 + k_1(\mathbf{x}_1, \mathbf{x}'_1) + k_2(\mathbf{x}_2, \mathbf{x}'_2) + k_1(\mathbf{x}_1, \mathbf{x}'_1)k_2(\mathbf{x}_2, \mathbf{x}'_2),$$

where $\mathbf{x}_l, \mathbf{x}'_l \in \mathcal{X}_l$ for $l = 1, 2$, is a positive definite kernel.

2. Centring of kernels.

2.1. Reproducing kernel Hilbert space. Recall that Hilbert space is a complete inner product space equipped with a positive definite inner product. Let \mathcal{H} be a Hilbert space of functions over a set \mathcal{X} with an inner product $\langle \cdot, \cdot \rangle_{\mathcal{H}}$. The Hilbert space \mathcal{H} is called a reproducing kernel Hilbert space (RKHS) if and only if there exists a function $k : \mathcal{X} \times \mathcal{X} \rightarrow \mathbb{R}$ satisfying

1. $k(x, \cdot) \in \mathcal{H}$ for all $x \in \mathcal{X}$
2. $f(x) = \langle f, k(x, \cdot) \rangle_{\mathcal{H}}$ for all $f \in \mathcal{H}$ and $x \in \mathcal{X}$

The function k is called reproducing kernel. Note that using the two properties, we have that $k(x, x') = \langle k(x, \cdot), k(x', \cdot) \rangle_{\mathcal{H}}$, hence k is positive definite. It can be shown by the Moore–Aronszajn theorem (?) that a kernel defines a unique RKHS and vice versa. We write the norm of a function f in \mathcal{H} as $\|f\|_{\mathcal{H}} = \sqrt{\langle f, f \rangle}$.

2.2. *Centring of kernel and functions in RKHS.* Let P be distribution over a non-empty set \mathcal{X} and $X, X' \in \mathcal{X}$ are independent and follow P . We consider a kernel k on \mathcal{X} and let \mathcal{H}_k denote the RKHS induced by k . We can center this kernel by,

$$k_{cent}(x, x') = \langle k(x, \cdot) - \mu_P, k(x', \cdot) - \mu_P \rangle_{\mathcal{H}_k} \quad (2.1)$$

where μ_P is the kernel mean given by

$$\mu_P := \mathbb{E}_{X \sim P} [k(X, \cdot)] = \int_{\mathcal{X}} k(x, \cdot) dP(x).$$

Note that the expectation of any function $f \in \mathcal{H}_k$ can be computed as an inner product with μ_P :

$$\begin{aligned} \mathbb{E}_{X \sim P} [f(X)] &= \int_{\mathcal{X}} f(x) dP(x) \\ &= \int_{\mathcal{X}} \langle k(x, \cdot), f \rangle_{\mathcal{H}_k} dP(x) \\ &= \left\langle \int_{\mathcal{X}} k(x, \cdot) dP(x), f \right\rangle_{\mathcal{H}_k} = \langle \mu_P, f \rangle_{\mathcal{H}_k}. \end{aligned}$$

The centred kernel (2.1) is positive definite by construction. We can see that this corresponds with (2.9) in the main paper by

$$\begin{aligned} \langle k(x, \cdot) - \mu_P, k(x', \cdot) - \mu_P \rangle_{\mathcal{H}_k} &= \langle k(x, \cdot), k(x', \cdot) \rangle_{\mathcal{H}_k} - \langle \mu_P, k(x', \cdot) \rangle_{\mathcal{H}_k} - \langle k(x, \cdot), \mu_P \rangle_{\mathcal{H}_k} + \langle \mu_P, \mu_P \rangle_{\mathcal{H}_k} \\ &= k(x, x') - \mathbb{E}_{X \sim P} [k(x', X)] - \mathbb{E}_{X' \sim P} [k(X', x)] + \mathbb{E}_{X, X' \sim P} [k(X, X')]. \end{aligned}$$

Note that

$$\begin{aligned} \mathbb{E}_{X, X' \sim P} [k(X, X')] &= \int_{\mathcal{X}} \int_{\mathcal{X}} k(x, x') dP(x) dP(x') \\ &= \int_{\mathcal{X}} \int_{\mathcal{X}} \langle k(x, \cdot), k(x', \cdot) \rangle_{\mathcal{H}_k} dP(x) dP(x') \\ &= \left\langle \int_{\mathcal{X}} k(x, \cdot) dP(x), \int_{\mathcal{X}} k(x', \cdot) dP(x') \right\rangle_{\mathcal{H}_k} = \langle \mu_P, \mu_P \rangle_{\mathcal{H}_k}. \end{aligned}$$

Given a sample x_1, \dots, x_n drawn from P , the kernel mean μ_P can be estimated empirically, by

$$\hat{\mu}_P = \frac{1}{n} \sum_{i=1}^n k(x_i, \cdot).$$

By replacing μ_P with $\hat{\mu}_P$, we get (2.10) of the main paper.

3. Kronecker products.

3.1. Kronecker product and its properties.

Kronecker product. Consider two matrices $\mathbf{A} = \{a_{i,j}\}_{1 \leq i \leq n, 1 \leq j \leq m}$ and $\mathbf{B} = \{b_{i,j}\}_{1 \leq i \leq p, 1 \leq j \leq q}$. The Kronecker product of the two matrices, $\mathbf{A} \otimes \mathbf{B}$, is the matrix of size $np \times mq$ given by

$$\mathbf{A} \otimes \mathbf{B} = \begin{bmatrix} a_{1,1}\mathbf{B} & \dots & a_{1,m}\mathbf{B} \\ \vdots & \ddots & \vdots \\ a_{n,1}\mathbf{B} & \dots & a_{n,m}\mathbf{B} \end{bmatrix}$$

More generally, we denote the Kronecker product of $d \geq 2$ matrices, \mathbf{A}_l where $l = 1, \dots, d$ by

$$\mathbf{A} := \bigotimes_{l=1}^d \mathbf{A}_l$$

If each matrix \mathbf{A}_l is size $n_l \times m_l$, the resulting Kronecker product matrix \mathbf{A} has size $\prod_{l=1}^d n_l \times \prod_{l=1}^d m_l$.

Kronecker product properties. We list some of the properties of Kronecker product that we use in this paper. In addition to \mathbf{A}_l defined above, let us assume we have, for $l = 1, \dots, d$, \mathbf{B}_l of size $p_l \times q_l$, \mathbf{B}'_l of size $p_l \times q_l$, \mathbf{C}_l of size $h_l \times k_l$ and \mathbf{D}_l of size $m_l \times p_l$. The size of matrices is given so that the operations $\mathbf{B}_l + \mathbf{B}'_l$ and $\mathbf{A}_l \mathbf{D}_l \mathbf{B}_l$ are allowed.

1. Bilinearity:

$$\mathbf{A}_l \otimes (\mathbf{B}_l + \mathbf{B}'_l) = \mathbf{A}_l \otimes \mathbf{B}_l + \mathbf{A}_l \otimes \mathbf{B}'_l$$

2. Associativity:

$$\begin{aligned} \mathbf{A}_l \otimes (\mathbf{B}_l \otimes \mathbf{C}_l) &= (\mathbf{A}_l \otimes \mathbf{B}_l) \otimes \mathbf{C}_l \\ \alpha(\mathbf{A}_l \otimes \mathbf{B}_l) &= (\alpha \mathbf{A}_l) \otimes \mathbf{B}_l = \mathbf{A}_l \otimes (\alpha \mathbf{B}_l) \end{aligned}$$

where α is a scalar.

3. Transpose:

$$\left(\bigotimes_{l=1}^d \mathbf{A}_l \right)^\top = \bigotimes_{d=l}^d \mathbf{A}_l^\top$$

4. Inverse:

$$\left(\bigotimes_{l=1}^d \mathbf{A}_l \right)^{-1} = \bigotimes_{d=l}^d \mathbf{A}_l^{-1}$$

5. The mixed product properties:

$$\bigotimes_{l=1}^d (\mathbf{A}_l \mathbf{D}_l) = \left(\bigotimes_{l=1}^d \mathbf{A}_l \right) \left(\bigotimes_{l=1}^d \mathbf{D}_l \right)$$

This can be generalised further. For example,

$$\bigotimes_{l=1}^d (\mathbf{A}_l \mathbf{D}_l \mathbf{B}_l) = \left(\bigotimes_{l=1}^d \mathbf{A}_l \right) \left(\bigotimes_{l=1}^d \mathbf{D}_l \right) \left(\bigotimes_{l=1}^d \mathbf{B}_l \right)$$

6. Matrix vector product

$$(\mathbf{A}_l \otimes \mathbf{B}_l) \mathbf{v} = \text{vec} \left(\mathbf{B}_l \mathbf{V} \mathbf{A}_l^\top \right)$$

where $\mathbf{V} = \text{vec}^{-1}(\mathbf{v})$ is the inverse of the vectorization operator and \mathbf{v} is a vector of length $m_l q_l$.

3.2. *Eigendecomposition of a Gram matrix with Kronecker product.* Assume a tensor product kernel

$$k(\mathbf{x}, \mathbf{x}') = \prod_{l=1}^d k_d(\mathbf{x}_l, \mathbf{x}'_l)$$

over a multidimensional grid $\mathcal{X} = \mathcal{X}_1 \times \dots \times \mathcal{X}_d$ where $\mathbf{x}_l \in \mathcal{X}_l$ and each k_l is defined on \mathcal{X}_l . Let n_l denote the dimension of each grid. Then the associated Gram matrix can be written as

$$\mathbf{K} = \bigotimes_{l=1}^d \mathbf{K}_l$$

where \mathbf{K}_l is a $n_l \times n_l$ gram matrix for l input dimension, with i, j -th element given by $k_l(\mathbf{x}_{(l),i}, \mathbf{x}_{(l),j})$. Let $\mathbf{K}_l = \mathbf{Q}_l \mathbf{\Lambda}_l \mathbf{Q}_l^\top$ be eigendecomposition of each matrix. Then the eigendecomposition of the matrix \mathbf{K} is the following:

$$\begin{aligned} \mathbf{K} &= \bigotimes_{l=1}^d \left(\mathbf{Q}_l \mathbf{\Lambda}_l \mathbf{Q}_l^\top \right) \\ &= \bigotimes_{l=1}^d \mathbf{Q}_l \bigotimes_{l=1}^d \mathbf{\Lambda}_l \bigotimes_{l=1}^d \mathbf{Q}_l^\top. \end{aligned} \quad (3.1)$$

Note that $\mathbf{Q} \equiv \bigotimes_{l=1}^d \mathbf{Q}^l$ is orthonormal, i.e., $\mathbf{Q}\mathbf{Q}^\top = \mathbf{I}_n$. We can confirm this by

$$\begin{aligned} \mathbf{Q}\mathbf{Q}^\top &= \left(\bigotimes_{l=1}^d \mathbf{Q}_l \right) \left(\bigotimes_{l=1}^d \mathbf{Q}_l \right)^\top = \left(\bigotimes_{l=1}^d \mathbf{Q}_l \right) \left(\bigotimes_{l=1}^d \mathbf{Q}_l^\top \right) \\ &= \bigotimes_{l=1}^d \mathbf{Q}_l \mathbf{Q}_l^\top = \bigotimes_{l=1}^d \mathbf{I}_{n_l} = \mathbf{I}_n. \end{aligned}$$

3.2.1. *An example with fractional Brownian motion kernel.* This decomposition leads to a particularly efficient algorithm when using fBM kernel or squared fBM kernel with a known Hurst coefficient γ_l . Let each k_l be a fBM_{γ_l} kernel. This means that we have only one hyper-parameter (scale parameter) to estimate for each dimension l . We denote the corresponding gram matrix by $\mathbf{K}_l = \alpha_l \mathbf{K}'_l$ where \mathbf{K}'_l is un-scaled gram matrix. Let $\mathbf{K}'_l = \mathbf{Q}_l \mathbf{\Lambda}_l \mathbf{Q}_l^\top$ be the eigendecomposition of the un-scaled matrix. Then eigendecomposition of \mathbf{K}_l is

$$\mathbf{K}_l = \alpha_l \mathbf{K}'_l = \mathbf{Q}_l (\alpha_l \mathbf{\Lambda}_l) \mathbf{Q}_l^\top.$$

Using (3.1), we can write

$$\mathbf{K} = \bigotimes_{l=1}^d \mathbf{K}'_l = \bigotimes_{l=1}^d \mathbf{Q}_l \bigotimes_{l=1}^d (\alpha_l \mathbf{\Lambda}_l) \bigotimes_{l=1}^d \mathbf{Q}_l^\top.$$

This means that when estimating the hyper-parameters by maximising the marginal likelihood or by MCMC, we do not have to apply eigendecomposition at each iteration. By simply multiplying each eigenvalue by the scale parameters, the inverse and the determinant can be updated.

3.3. *Row-wise Kronecker product.* Consider two matrices $\mathbf{A} = \{a_{i,j}\}_{1 \leq i \leq n, 1 \leq j \leq m}$ and $\mathbf{B} = \{b_{i,j}\}_{1 \leq i \leq n, 1 \leq j \leq q}$. Let \mathbf{A}_i and \mathbf{B}_i be the i -th row of the matrices \mathbf{A} and \mathbf{B} respectively. The row-wise Kronecker product of the two matrices, $\mathbf{A} \bullet \mathbf{B}$, is the matrix of size $n \times mq$ given by

$$\mathbf{A} \bullet \mathbf{B} = \begin{bmatrix} \mathbf{A}_1 \otimes \mathbf{B}_1 \\ \mathbf{A}_2 \otimes \mathbf{B}_2 \\ \vdots \\ \mathbf{A}_n \otimes \mathbf{B}_n \end{bmatrix}$$

where \otimes is Kronecker product. Row-wise Kroncker product may also be called face-splitting product. Let \mathbf{v} be a vector of length n . Then we have

$$\mathbf{A} \bullet \mathbf{v} = \mathbf{v} \bullet \mathbf{A} = \mathbf{V}_d \mathbf{A}$$

where $\mathbf{V}_d = \text{diag}(\mathbf{v})$, a diagonal matrix with its diagonal elements given by \mathbf{v} .